# Study of Molecular Conductors by X-ray Diffuse Scattering

Sylvain Ravy

*Laboratoire de physique des solides, bât. 510, Université Paris-sud, 91405 Orsay Cedex, France, and Synchrotron SOLEIL, L'Orme des merisiers, Saint-Aubin BP 48, 91192 Gif-sur-Yvette Cedex, France*†

*Received March 2, 2004*

## *Contents*



## *1. Introduction*

Small deviations to perfect periodicity can have a large influence on physical properties of crystals. The color of minerals and the plasticity of metals, which are prominent macroscopic properties, are due to impurities and dislocations, which are microscopic structural modifications. Among the techniques giving access to such small structural changes, X-ray diffraction has an important place. Not only does X-ray diffraction allow one to obtain the average structure of materials, that is, the position of the atoms in the unit cell, but it can also give valuable information on tiny modifications of these positions, through the study of out-of-Bragg scattering. This scattering comes *either* from long-range-ordered phases, whose structural properties are very close to those of the parent phase, *or* from short-range order originating from pretransitional fluctuations or disorder and giving rise to the so-called *diffuse scattering*. This review is devoted to the study of molecular conductors by these methods.

In section 2, the basics of diffraction will be recalled, following the best textbooks in the field.[1−4] Special attention will be paid to distinguish between the phenomena giving rise to small additional scattering features, the displacement and the substitution disorder, and their potential coupling. The effects of pretransitional fluctuations on the scattering will be simply recalled.

Sylvain Ravy was born on April 26, 1961, in Quimper, France. He graduated as an engineer from École Supérieure d'Électricité and received his Ph.D. degree from the University Paris-sud on the "study of structural instabilities in organic conductors" under the guidance of Jean-Paul Pouget at Laboratoire de Physique des Solides, where he was researcher at the Centre National de la Recherche Scientifique (CNRS). From 1995 to 1997 he was visiting scientist at University of Wisconsin—Milwaukee, where he learned electron spectroscopy methods. He is a part time teacher at Orsay University and currently am in charge of the development of a diffraction beamline called CRISTAL at the new synchrotron radiation center SOLEIL, in construction at Saint Aubin, near Paris, France.

† Current address.

10.1021/cr030662h CCC: $48.50 
Published on Web 10/27/2004

Since the first diffuse scattering studies performed on TTF-TCNQ,[5,6] which provided evidence for the Peierls instability, many original structural phase transitions have been observed in molecular conductors, which are mainly due to their one-dimensional (1D) character. For that reason, section 3 will be devoted to the 1D physics, with special emphasis on the many ground states newly discovered, involving complicated mixing of 1D order parameters. Especially important is the role of the electron−phonon coupling and the electronic interactions to interpret these phases. A brief introduction of the Bechgaard and the Fabre salts (the $(TM)_2X$ family) will be given in section 4, before presenting the charge-density wave-like instabilites, the anion ordering (AO) transitions, and the mixed states observed in the 2:1 charge-transfer salts. In this respect, this review will attempt to complete with new results the already published reviews on the structural instabilities of the TTF-TCNQ family[7] and the Bechgaard salts.[8]

Section 5 will focus on the effects of disorder on the structural properties of molecular conductors. The trivial fact that the building blocks of these materials are heavy molecules and not atoms makes easier the observation of disorder by diffuse scattering. This property allows one to improve our knowledge of the disorder in these materials. In this respect, a clear demonstration of the existence of strong pinning in charge-density wave systems can be obtained in molecular systems, while it is much more difficult in other charge-density wave (CDW) systems. The possibility to control the amount of disorder is another asset of molecular conductors. This made it possible to study and differentiate the effect of anions or molecules on phase transitions in the solid solutions of charge-transfer salts.

All these results show that very small modifications of either molecules or external parameters can lead to completely different ground states. That is the reason for the richness of the molecular conductors phase diagrams that every researcher in the field knows.

## 2. X-ray Diffuse Scattering

### 2.1. X-ray Diffraction

When an X-ray beam impinges on matter, two scattering processes occur. The incoherent Compton scattering, in which electrons recoil due to the photon impact, and the Thomson scattering, which is the coherent scattering process of X-rays with matter. Only Thomson scattering gives rise to interferences. Due to the weak interaction between X-ray photons and electrons, multiple scattering and the scattered intensity with respect to the direct incident beam can be neglected. This approximation, called the kinematic approximation, allows one to relate the total electron density $\rho_e(\mathbf{r})$ at the instantaneous positions $\mathbf{r}$ to the differential scattering cross section $(d\sigma/d\Omega)$ by the use of a Fourier transform (FT):

$$\frac{d\sigma}{d\Omega} = |b_{th}\int \rho_e(\mathbf{r}) \exp(-i\mathbf{Q}\cdot\mathbf{r}) d^3\mathbf{r}|^2 \qquad (2.1)$$

In this expression, $b_{th} = 2.8 \times 10^{-15}$ m is the Thomson scattering length, $\mathbf{Q}$ is the scattering wave vector, equal to the difference between the incident wave vector and the scattered wave vector, and the quantity expressed by the integral is the scattered amplitude $A(\mathbf{Q})$. This quantity is related to the total electron density by a Fourier transform, a linear transformation which makes the scattering calculation tractable. In the case of a single atom, the scattered amplitude is called the scattering factor, noted $f(\mathbf{Q})$. Note that, in the previous calculation, we have implicitly assumed that X-rays are elastically scattered, which is not strictly true: atoms are moving and scatter X-rays inelastically. However, X-ray frequencies are much larger ($\sim 2 \times 10^{18}$ Hz for 8 keV photons) than typical atomic vibration frequencies ($\sim$10 THz), so that in most experiments the frequency shifts are not observable. This *energy integration* of most X-ray detectors means that the scattering cross section is in fact related to an equal time correlation function, as eq 2.1 implicitly assumes.

Let us now consider a perfect crystal, that is, a crystal in which the $N$ unit cells at position $\mathbf{R}_{uvw} = u\mathbf{a} + v\mathbf{b} + w\mathbf{c}$ are identical and contain atom $i$ of scattering factor $f_j$ at position $\mathbf{r}_j$. The scattered amplitude reads

$$A(\mathbf{Q}) = (\sum_j f_j \exp(-i\mathbf{Q}\cdot\mathbf{r}_j)) \sum_{uvw} \exp(-i\mathbf{Q}\cdot\mathbf{R}_{uvw}) \equiv F(\mathbf{Q})\Sigma(\mathbf{Q}) \qquad (2.2)$$

where $F(\mathbf{Q})$ is the structure factor of the unit cell and $\Sigma(\mathbf{Q})$ is the form factor of the crystal. For large enough crystals, this latter quantity is nonzero only if

$$\mathbf{Q} = \mathbf{Q}_{hkl} \equiv h\mathbf{a}^* + k\mathbf{b}^* + l\mathbf{c}^* \qquad (2.3)$$

where $\mathbf{a}^*$, $\mathbf{b}^*$, and $\mathbf{c}^*$ are the reciprocal lattice basis vectors, defined by the well-known relations $\mathbf{a}^*\cdot\mathbf{a} = 2\pi$, $\mathbf{a}^*\cdot\mathbf{b} = 0$, etc. When this condition is fulfilled, all unit cells scatter *in phase*, resulting in a phenomenon called *diffraction*. Intense X-ray beams are diffracted in special directions, giving rise to *Bragg spots* on 2D detectors, whose intensity is proportional to $|F(\mathbf{Q})|^2$. Measuring the integrated intensity of the maximum number of these spots allows one to retrieve the unit cell content. And when the quality of the data is very good, the *electron density* of the unit cell can be retrieved.[9] This is the work of crystallographers.

### 2.2. Diffuse Scattering

However, perfection is not from our world. Even in the best crystals such as silicon, the atoms are moving around due to temperature, which causes *displacement disorder*. In alloys or solid solutions, sites may be occupied by different species, which causes *substitution disorder*. In both cases, the scattered amplitude reads

$$A(\mathbf{Q}) = \sum_n F_n(\mathbf{Q}) \exp(-i\mathbf{Q}\cdot\mathbf{R}_n) \qquad (2.4)$$

where $F_{uvw} \equiv F_n$ now depends on the instantaneous

content of the unit cell located at $\mathbf{R}_{uvw} = u\mathbf{a} + v\mathbf{b} + w\mathbf{c}$. The classical way to deal with this disorder problem is to express the structure factor as

$$F_n(\mathbf{Q}) = \langle\langle F_n(\mathbf{Q})\rangle_n\rangle_t + \phi_n(\mathbf{Q}) \quad (2.5)$$

where $\langle\langle ...\rangle_n\rangle_t$ indicates the spatial and time average. Note that the recent use of coherent X-rays in synchrotron radiation experiments[10] allows one to measure intensity variations in the millisecond or even microsecond time range. This makes the time average only effective in the fast time region (<1 ms). This is not the case in the studies reviewed here, and the averages will be simply noted by $\langle ...\rangle$.

Substituting formula 2.4 in eq 2.1 with the use of the above definition gives that the scattered intensity is related to the FT of the pair correlation function:

$$\langle F_n^*(\mathbf{Q})F_{n+m}(\mathbf{Q})\rangle = |\langle F(\mathbf{Q})\rangle|^2 + \langle \phi_n^*(\mathbf{Q})\phi_{n+m}(\mathbf{Q})\rangle \quad (2.6)$$

The FT of the first term of this equation is the term of *diffraction*, which gives the intensity of the Bragg spots. It is due to the *long-range order* (LRO) present in the crystal. The effect of disorder on this intensity manifests itself by the presence of the structure factor average $\langle F(\mathbf{Q})\rangle$. The most famous consequence is that due to thermal agitation the atoms have a scattering factor $f\exp(-M)$, where $\exp(-M)$ is the Debye−Waller factor. This leads to a decrease of the intensity by a factor $\exp(-2M)$.

The FT of the second term of eq 2.6 is the *diffuse scattering* term. Its existence is due to the *short-range order* (SRO) present in the crystal. As the total number of electrons is the same in a disordered crystal, the decrease of the Bragg reflection intensity is compensated by the increase of this scattering, usually not localized in the reciprocal space. The intensity $I_{DD}(\mathbf{Q})$ of the diffuse scattering is given by

$$I_{DD}(\mathbf{Q}) = N\sum_m \langle \phi_n^*(\mathbf{Q})\phi_{n+m}(\mathbf{Q})\rangle \exp(-i\mathbf{Q}\cdot\mathbf{R}_m) \quad (2.7)$$

It is clear from this expression that only *deviation* from the perfect periodicity ($\phi_n \neq 0$) gives rise to diffuse scattering. The study of this diffusion allows one to study the disorder in materials.

## 2.3. Another Expression of the Diffuse Scattering Intensity

Another expression of the diffuse scattering, due to Krivoglaz,[4] is very useful to deal with complex cases of disorder, especially when substitution and displacement disorders are coupled, as we will see in section 5.

Let us consider a crystal containing two kinds of atoms A and B, with scattering factors $f_A$ and $f_B$, in concentrations $c$ and $1 - c$, respectively. The substitution disorder is described by the variable $\sigma_n$, which is equal to 1 if site $n$ is occupied by atom A and 0 otherwise. The atoms are displaced by the quantity $\mathbf{u}_n$. The scattering amplitude then reads

$$A(\mathbf{Q}) = \sum_n (\Delta f\,(\sigma_n - c) + \bar{f})e^{i\mathbf{Q}\cdot\mathbf{R}_n}e^{i\mathbf{Q}\cdot\mathbf{u}_n} \quad (2.8)$$

where $\Delta f = f_A - f_B$ is the *contrast* term and $\bar{f} = cf_A - (1 - c)f_B$ is the average structure factor. The final expression of the scattered amplitude is obtained by using the Fourier series of $\sigma_n - c$ and $\mathbf{u}_n$:

$$\mathbf{u}_\mathbf{q} = \sum_n \mathbf{u}_n e^{i\mathbf{q}\mathbf{R}_n}; \quad \sigma_\mathbf{q} = \sum_n (\sigma_n - c)e^{i\mathbf{q}\cdot\mathbf{R}_n} \quad (2.9)$$

After some algebra,[4,11,12] the intensity at the $\mathbf{Q}_{hkl} + \mathbf{q}$ reciprocal position reads

$$I(\mathbf{Q} = \mathbf{Q}_{hkl} + \mathbf{q}) = \langle|\Delta f\sigma_\mathbf{q} + i\bar{f}\mathbf{Q}\cdot\mathbf{u}_\mathbf{q}|^2\rangle_t \quad (2.10)$$

This important formula allows one to clearly differentiate the effects of the different types of disorder and their coupling.

The first term

$$I_{\mathrm{sub}}(\mathbf{Q} = \mathbf{Q}_{hkl} + \mathbf{q}) = \Delta f^2\langle\sigma_\mathbf{q}\sigma_{-\mathbf{q}}\rangle_t \quad (2.11)$$

gives the intensity scattered in the case of a pure substitution disorder. If there is no correlation between the A and B positions, which is very rare in metals but observable in molecular systems (see section 5), this expression reduces to $c(1 - c)\Delta f^2$. It is called the Laue formula because Max von Laue was the first to calculate this expression in the 1920s,[1] at a time when diffuse scattering had still not been observed. As expected, $I_{\mathrm{sub}}$ cancels out when the order is back, that is, when $c = 0$ (no B atoms), $c = 1$ (no A atoms), or the contrast term $\Delta f$ is zero (A = B). This scattering is maximum at *small angles*.

The second term

$$I_{\mathrm{dis}}(\mathbf{Q} = \mathbf{Q}_{hkl} + \mathbf{q}) = \bar{f}^2\langle|\mathbf{Q}\cdot\mathbf{u}_\mathbf{q}|^2\rangle_t \quad (2.12)$$

gives the intensity scattered when a displacement disorder alone is present. Each displacement mode of wave vector $\mathbf{q}$ gives additional scattering at $\pm\mathbf{q}$ from the Bragg reflections. This obviously applies to thermal agitation. Qualitatively, it can be said that each phonon of wave vector $\mathbf{q}$ participates at $\pm\mathbf{q}$ to the cloud of diffuse scattering located around each Bragg reflection. Through the scalar product $\mathbf{Q}\cdot\mathbf{u}_\mathbf{q}$, the displacive term is proportional to the amplitude of displacement squared, $u_\mathbf{q}^2$, and the scattering vector squared, $Q^2$. This means that this diffuse scattering is *not* observable at small angles.

The third term

$$I_{\mathrm{A}}(\mathbf{Q} = \mathbf{Q}_{hkl} + \mathbf{q}) = -2\bar{f}\Delta f\,\mathrm{Im}\langle\sigma_{-\mathbf{q}}\mathbf{Q}\cdot\mathbf{u}_\mathbf{q}\rangle_t \quad (2.13)$$

arises from the coupling between the substitution and the displacement disorders. Indeed, this term cancels out when the atomic displacements are independent of the species ($\sigma_{-\mathbf{q}}\mathbf{u}_\mathbf{q} \sim \sum_m\langle\sigma_n - c\rangle\langle\mathbf{u}_{n+m}\rangle e^{i\mathbf{q}\cdot\mathbf{R}_m} = 0$). Contrary to the two previous terms, $I_{\mathrm{A}}$ has a very particular symmetry property which makes it unique in diffraction theory:

$$I_{\mathrm{A}}(\mathbf{Q}_{hkl} + \mathbf{q}) = -I_{\mathrm{A}}(\mathbf{Q}_{hkl} - \mathbf{q}) \quad (2.14)$$

This means that $I_{\mathrm{A}}$ is asymmetric with respect to the associated $\mathbf{Q}$-Bragg reflection. This asymmetric effect has been discovered in aluminum alloys containing

Guinier−Preston zones.[13] Indeed in this case, the substituent atoms (e.g. Ag or Zn) regroup in small clusters having a slightly different lattice parameter. This originates the displacements/substitution coupling. This effect has been differently explained in textbooks.[2,3] However, there is an elegant way to understand it, based on the holographic diffraction concept[14,15] explained in section 5.4.

## 2.4. Phase Transitions

Structural phase transitions are common in molecular materials; it is then useful to rephrase the expression of the scattered intensity by using the classical concepts of phase transitions.[16] Second-order phase transitions are described by the temperature behavior of an order parameter $\eta_{\mathbf{q}c}$, which is zero above the transition temperature $T_c$ and nonzero below. $\mathbf{q}_c$ is the critical wave vector or propagation vector, which characterizes the new type of LRO stabilized below $T_c$. In the simplest case, the local order parameter at position $\mathbf{r}_n$ reads

$$\eta_{\mathbf{q}c}(\mathbf{r}_n) = \eta_{\mathbf{q}c} \cos(\mathbf{q}_c \cdot \mathbf{r}_n + \phi)$$

In the case of a displacive phase transition, the order parameter is the amplitude $u_{\mathbf{q}c}$ of a displacive mode. For an order−disorder phase transition, the local order parameter can be defined as the deviation of the average occupation of site $\mathbf{r}_n$ by A from its average value $c$, that is, $\langle\sigma_n\rangle - c$. The amplitude $\langle\sigma_{\mathbf{q}c}\rangle$ of this quantity is the order parameter. To go further, one has to use the fluctuation−dissipation theorem, which relates the fluctuations of the order parameter to the response function or generalized susceptibility $\chi(\mathbf{q})$. In Fourier space, this theorem reads

$$\langle\eta_{\mathbf{q}}\eta_{-\mathbf{q}}\rangle - \langle\eta_{\mathbf{q}}\rangle\langle\eta_{-\mathbf{q}}\rangle = k_B T\chi(\mathbf{q}) \qquad (2.15)$$

It is easy to see that for both types of phase transitions (displacive or order−disorder) the scattered intensity, given by eqs 2.11 and 2.12, is expressed as

$$I(\mathbf{Q}_{hkl} \pm \mathbf{q}) = I(\mathbf{q}) \sim k_B T\chi(\mathbf{q}) + \langle\eta_{\mathbf{q}}\rangle\langle\eta_{-\mathbf{q}}\rangle \qquad (2.16)$$

This means that, below the phase transition, the new long-range order induces new spots in the scattering pattern, usually called satellite reflections. These reflections are located at $\pm\mathbf{q}_c$ of the main Bragg reflection, and their intensities are proportional to the square of the order parameter $\langle\eta_{\mathbf{q}}\rangle = \eta_{\mathbf{q}c}$.

Above the phase transition only fluctuations survive ($\langle\eta_{\mathbf{q}}\rangle = 0$). (Fluctuations are indeed present below $T_c$ and give diffuse scattering around the satellite reflections.) These fluctuations give rise to diffuse scattering (there is only SRO) whose intensity is proportional to $T\chi(\mathbf{q})$. $I(\mathbf{q})/T$ versus $T$ plots give the temperature dependence of the susceptibility $\chi(\mathbf{q})$ (see examples in Figures 9 and 10). In a mean-field Landau−Guinzburg approach, this response function reads

$$\chi(\mathbf{q}) = \frac{\chi(\mathbf{q}_c)}{1 + (\xi_x q_x)^2 + (\xi_y q_y)^2 + (\xi_z q_z)^2} \qquad (2.17)$$

where $\xi_i$ are the *correlation lengths* in the $i$ directions, which diverge at the phase transition. In this approximation, the diffuse scattering has a Lorentzian (Ornstein−Zernike) line shape, whose half-widths at half-maximum (hwhm) are equal to $\xi$. This line shape is usually in good agreement with measurements. In the real space, it means that the correlation function of the order parameter follows

$$\langle\eta(0)\eta(r)\rangle \sim \frac{1}{r}\exp(-r/\xi) \qquad (2.18)$$

in an isotropic case.

More sophisticated theories of phase transition, beyond the scope of this introduction, are however needed to interpret high-resolution diffuse scattering measurements close to $T_c$.[16] This *critical* regime, however, can be studied by scattering measurements, and thermodynamic quantities such as the order parameter, the generalized susceptibility, and the correlation lengths can be measured by X-ray diffraction experiments. Let us recall that, for second-order phase transitions, the critical exponents $\beta$, $\gamma$, and $\nu$ can be defined to describe the power-law behavior of the three previous quantities as a function of the reduced temperature $t = (T - T_c)/T_c$ close to $T_c$.

$$\eta_{\mathbf{q}c} \sim |t|^{\beta} \quad \text{for} \quad T < T_c \qquad (2.19)$$

$$\chi(0) \sim |t|^{-\gamma} \quad \text{and} \quad \xi \sim |t|^{-\nu} \quad \text{for} \quad T > T_c \qquad (2.20)$$

When the systems are very anisotropic, as is the case for low-dimensional materials, the diffuse scattering presents unique features easily shown by eq 2.17. For example, in purely 1D systems running in direction **b**, there is no transverse correlation and consequently $\xi_x = \xi_z = 0$. $\chi(\mathbf{q})$ has no structure in the corresponding directions and is geometrically represented by a diffuse sheet of width $\xi_y^{-1}$ in the reciprocal space. This diffuse sheet gives rise to diffuse lines on X-ray photographs, as exemplified Figure 12. These lines are typical of 1D instabilities.

Interestingly enough, the behavior of $\chi(\mathbf{q})$ is related to the forces which trigger the phase transition. To illustrate this idea, let us consider the simple Ising model. Many systems containing spins or nonsymmetric molecules (pseudospins) can be modeled by a Ising model, in which a pseudospin variable $S_i$ is 1 or −1 according to the + or − orientation of the pseudospin. The Ising Hamiltonian is

$$H = -\frac{1}{2}\sum_{i,j} J_{ij} S_i S_j \qquad (2.21)$$

where $J_{ij}$ is the energy difference between +...− and +...+ configurations. $J_{ij}$ can be directly calculated from the knowledge of the interacting potential between pseudospins. In the mean-field approximation, $\chi(\mathbf{q})$ simply reads

$$\chi(\mathbf{q}) = \frac{1}{k_B T - J(\mathbf{q})} \qquad (2.22)$$

where $J(\mathbf{q})$ is the Fourier transform of the $J_{ij}$ constants. In the case of first neighbor interactions

$$J(\mathbf{q}) = J_x \cos q_x a + J_y \cos q_y b + J_z \cos q_z c \quad (2.23)$$

Close to the phase transition, the combination of eqs 2.17 and 2.22 yields

$$\xi_x = a\sqrt{\frac{J_x}{2k_B(T - T_c)}} \quad (2.24)$$

which shows that the correlation lengths are directly related to the forces involved in the phase transition. The study of diffuse scattering gives access to interaction energies in a solid. This was done for example in molecular $C_{60}$.[17]

Finally, let us mention that, in the presence of impurities or defects coupled to the order parameter, the nature of the fluctuations is changed and the long-range order is generally lost. The term *quasi-phase transition* is used to described a situation in which, although no long-range order is actually observed, the behavior of an order parameter, which increases and saturates, can still be observed upon cooling. However, there is no unified description of the effect of disorder because many possible situations occur. In section 5, we will present cases where random fields or random bonds are pertinent to understand experiments at least qualitatively. Impurities can also pin the phase of the order parameter and give rise to spectacular asymmetry effects. This will be described in section 5.

## 3. Low-Dimensional Systems

### 3.1. Introduction to Organic Conductors

It is not the purpose of this paper to review the history of molecular conductors. Nevertheless, it should be said that the first molecular conductor studies clearly showed their connection to low-dimensional physics. Indeed, from the very beginning, chemists and physicists had to address the issues of 1D instabilities, either by studying them or by trying to bypass them.

The first organic conductor was obtained in 1954 by exposing perylene to bromine.[18] However, it is with the discovery of the acceptor TCNQ (tetracyanoquinone) in 1960[19] and the synthesis of the first conducting compounds such as Qn-(TCNQ) that the interest in this new type of materials awoke. TTF (tetrathiafulvalenium) was synthesized in 1972,[20] and then it associated to TCNQ in the famous TTF-TCNQ.[21,22] The room-temperature conductivity of TTF-TCNQ is 500 $(\Omega\ \mathrm{cm})^{-1}$ and exhibits a maximum at 60 K just before a metal−insulator transition, below which a *charge-density wave* state is stabilized. (Note that TTF-TCNQ is not the most simple CDW organic system. In fact, three structural transitions occur successively below 60 K, the first one corresponding to the Peierls transition mentioned here.[7]) This phase transition, called the *Peierls transition*, is an intrinsic consequence of the 1D nature of this compound and of many organic compounds.

Indeed, as most of the molecules of organic conductors are planar, they stack in a direction where their orbitals overlap. Such a chain, when it exists, can present metallic properties, given some conditions, which all influence the structural properties of the chain:

(1) Charge carriers have to be added—either electrons to LUMOs (lowest unoccupied molecular orbitals) or holes to HOMOs (highest occupied molecular orbitals). This can be achieved by a charge transfer either from an acceptor to a donor, such as in TTF-TCNQ, or from an inorganic anion $X^-$ (or a cation), such as, for example, in Bechgaard salts $(TMTSF)_2X$. Note that, in the latter case, new structural instabilities related to the anions will emerge, as will be discussed in section 4.1.

(2) The conduction bandwidth has to be larger (or of the same order of magnitude) than the Coulomb energy between electrons, to avoid electronic (Mott) localization. In organic conductors, the typical bandwidth is 0.5−1 eV. On the other hand, the direct Coulomb energy of two electrons separated by 3−7 Å (the size of typical inter- or intramolecular distances) is as large as 2−4 eV. However, as organic molecules are highly polarizable, the Coulomb interactions are screened and the Coulomb energy is estimated to be about 0.3−0.5 eV.[24] The similarity between the band and the Coulomb energies is responsible for the conducting properties of molecular conductors, but it gives rise to new instabilities which will be described in the following section.

(3) The crystal quality must be good, because 1D systems are very sensitive to disorder. The stabilization of a metallic state strongly depends on the quality of the order in the material. This will be discussed in section 5.

The previous conditions are generally fulfilled in organic conductors. However, as we already mentioned, it is known from Peierls[23] that a 1D electron gas is unstable at zero temperature with respect to the opening of a gap at the Fermi level. The Peierls state was discovered in 1973 in the Krogman salt $K_2Pt(CN)_4{\cdot}xH_2O$[25] and observed soon after in transition metal dichalcogenides,[26] molybdenum blue bronze $K_{0.3}MoO_3$,[27,28] or trichalcogenides such as $TaS_3$, $NbSe_3$, and $(TaSe_4)_2I$,[29] to quote a few examples. To get rid of this metal−insulator phase transition (and disregarding the interest in studying this fascinating phenomena), different strategies were used.

After the Peierls transition was discovered in TTF-TCNQ,[5,7] pressure was applied on the compound in order to increase intrastack contacts and consequently the dimensionality of the salts. These attempts failed in TTF-TCNQ, which still exhibits a Peierls transition up to 35 kbar,[30] but were successful in the Bechgaard $(TMTSF)_2X$,[31] the Fabre $(TMTTF)_2X$,[32,33] and the $M(dmit)_2$ salts.[35] In these series, the metal−insulator phase transition disappears under pressure, and a superconducting state is stabilized at higher pressure.[34]

Another approach, actually similar to the previous one, consisted of increasing the number of lateral atoms in the molecule, to maximize intrastack contacts and get more isotropic properties.[36] The mol-

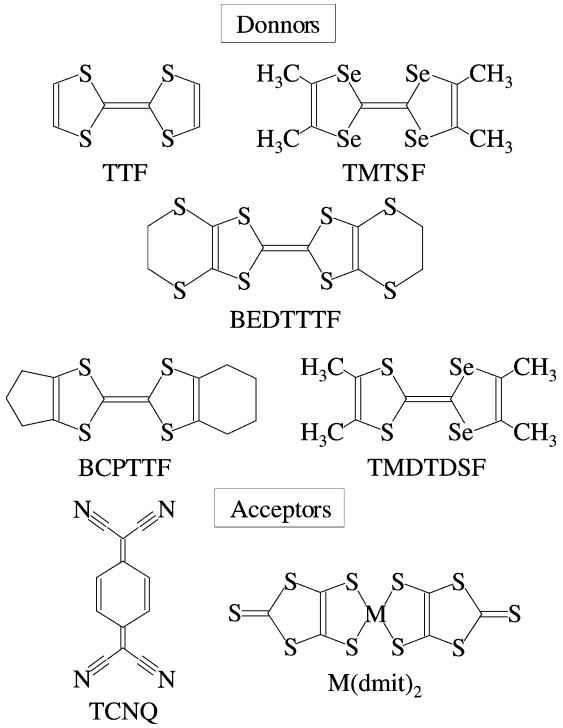


**Figure 1.** Examples of donor and acceptor molecules.

ecule which first allowed us to synthesize 2D systems is BEDTTTF (bis(ethylenedithio)-TTF)[37,34] (see Figure 1). With the exception of a few systems such as $(BEDT\text{-}TTF)_2ReO_4$,[37,38] where Peierls-like metal–insulator transitions occur, structural 1D instabilities are rare in this series. Indeed, phases in which the BEDT-TTF molecules regroup in pairs are numerous in BEDT-TTF systems, which renders this systems more 2D than other molecular conductors. These phases have the highest temperatures of superconductivity so far ($T_c = 12.8$ K at 0.3 kbar in $\kappa$-$(BEDT\text{-}TTF)_2Cu[N(CN)_2]Cl$), if we exclude the $C_{60}$ phases. Hundreds of new molecules have been synthesized, but that is not the scope of this paper. Let us note that even if many new compounds have been discovered, old systems still hide their secrets.

## 3.2. Some Basic Theoretical Considerations

The physics of the 1D electron gas emerged in the late 1970s,[39,40] and its basic concepts are widely used to interpret experimental results. We will give here a simple presentation of the Peierls instability, its modification when Coulomb interactions are taken into account, and the effect of such phenomena on structural phase transitions.

### *3.2.1. The Peierls Instability*

The Peierls instability dominates 1D physics, even if all aspects of 1D systems cannot be explained with this concept. Let us consider a 1D energy band partly filled (Figure 2a). In one dimension the charge transfer $\rho$ and the Fermi wave vector $2k_F$ are simply related by $\rho = 2 \times 2k_F$. In 1955 Peierls showed[23] that at $T = 0$ K this 1D electron gas is unstable with respect to the opening of an energy gap $2\Delta$ at the Fermi level (Figure 2c). This instability is due to the

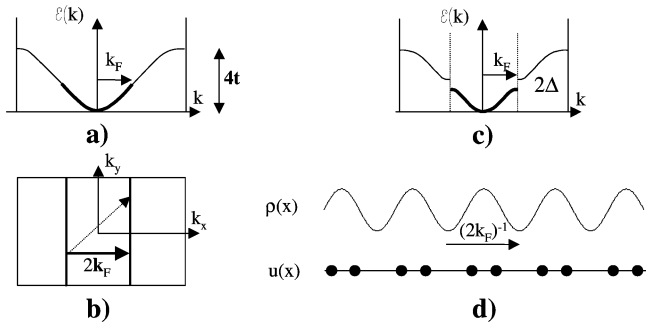


**Figure 2.** (a) Electronic band dispersion $\epsilon(k)$ of a 1D metal and (b) corresponding Fermi surface. The nesting wave vector is indicated. (c) Band dispersion in the Peierls state. (d) Schematic representation of a bond-order wave, consisting of a charge-density wave $\rho(x)$ and a lattice distortion $u(x)$ in quadrature.

divergence of the electron–hole response function or Lindhard function, which reads

$$\chi_e(\mathbf{q},T) = -\sum_k \frac{f(\epsilon(\mathbf{k})) - f(\epsilon(\mathbf{k}+\mathbf{q}))}{\epsilon(\mathbf{k}) - \epsilon(\mathbf{k}+\mathbf{q})} \qquad (3.1)$$

where $f(\epsilon(\mathbf{k}))$ is the Fermi–Dirac distribution function and $\epsilon(\mathbf{k})$ is the dispersive electronic energy. As it is well-known, this function diverges when part of the Fermi surface nests with another one after a translation of $\mathbf{q}$. In one dimension this is achieved when $\mathbf{q} = 2\mathbf{k}_F$, the *nesting* wave vector, but the concept is still valid for quasi-1D systems, and even some 2D systems.[42,43]

In the usual case, a resulting modulation of the electron density of wave vector $2k_F$, named the charge-density wave (CDW), is stabilized, associated with a periodic lattice distortion of same periodicity. This will be discussed later.

At the wave vector $2k_F$, the response function reads

$$\chi_e(2k_F,T) = N(E_F)\log(E_c/k_BT) \qquad (3.2)$$

where $N(E_F)$ is the density of electronic states at the Fermi level and $E_c$ is a cutoff energy close to the Fermi energy $E_F$. This expression clearly shows that $\chi_e(2k_F,T)$ diverges at $T = 0$ K, which is consistent with the Landau–Peierls theorem, which forbids any phase transition at finite temperature for 1D systems. Before considering the transverse interactions, which explain the occurrence of the Peierls transition at finite temperature, let us first discuss the essential role of the electron–phonon coupling.

In fact, pure CDWs are difficult to find (though an example will be given in section 3.2.4). What is usually called a CDW is the association of $2k_F$ charge and lattice modulations. In the classical Peierls mechanism, electrons respond to the perturbation caused by lattice vibrations, through the electron–phonon coupling. The easiest way to introduce the electron–phonon coupling is to make the electronic energy dependent on molecular positions $u_i$ or intramolecular deformations $v_i$. Starting from the following Hamiltonian

$$H = \sum_{i,\sigma} \epsilon n_{i,\sigma} + \sum_{i,\sigma} t(c^\dagger_{i,\sigma}c_{i+1,\sigma} + c_{i,\sigma}c^\dagger_{i+1,\sigma}) + H_{ph} \qquad (3.3)$$

where $c^{\dagger}_{i,\sigma}$ ($c_{i,\sigma}$) is the creation (annihilation) operator of a particle of spin $\sigma$ (+ or −) at site $i$, $n_{i,\sigma}$ is the density of spin $\sigma$ electrons at site $i$, $t$ is the transfer integral between two neighboring sites, and $\epsilon$ is the electronic site energy, the electron−phonon coupling terms simply read

$$\epsilon = \epsilon_0 + \beta v_i \tag{3.4}$$

$$t = t_0 + \alpha(u_{i+1} - u_i) \tag{3.5}$$

The first expression corresponds to the Holstein case,[44] while the second one is called SSH (Su−Schrieffer−Heeger)[45] and is the most common. $H_{ph}$ is the phonon Hamiltonian, whose analytical expression is model-dependent. It can be written here

$$H_{ph} = \frac{K_1}{2}\sum_i (u_{i+1} - u_i)^2 + \frac{K_2}{2}\sum_i v_i^2 \tag{3.6}$$

where $K_1$ and $K_2$ are elastic constants. Via the coupling constants $\alpha$ and $\beta$, phonons induce a perturbation on the electron gas, which responds through $\chi_e(2k_F,T)$ by modulating its charge-density at $2k_F$ in order to screen the perturbation. This screening softens a $2k_F$ phonon mode, which increases its amplitude and consequently the perturbation. This feedback corresponds to the classical description of the Peierls transition, which predicts the existence of a *soft mode* in the vicinity of a phase transition. Such a soft mode mechanism has been clearly observed in $K_2Pt(CN)_4Br_0{\cdot}3{\times}H_2O$[46] and the blue bronze $K_{0.3}MoO_3$[47] by inelastic neutron scattering (INS) but not in TTF-TCNQ, the only organic conductor studied by INS.[46] (In this case the soft mode does not go to zero frequency at the phase transition.[46]) Note that this soft mode mechanism is possible because electrons are faster than the phonon modes they have to screen. This corresponds to the *adiabatic limit*.

The nature of the stabilized lattice distortion depends on the type of coupling involved in the transition. In the SSH case, the low-temperature phase corresponds to a *bond-order wave* (BOW) because the transfer integral $t$ and, consequently, the intermolecular distances are modulated (see Figure 2d). This corresponds to most experimental situations. In the Holstein case, a *site* CDW is stabilized, in which the molecular charges are modulated and intramolecular modes are involved. BOWs and site CDWs do not have the same properties and can be in competition. In this section, we will use the notation **q**-BOW and **q**-CDW to note bond-order waves and site charge-density waves of wave vector **q**, respectively. In fact, the existence of mixed states in organic compounds makes this distinction necessary though cumbersome. Again, one has to keep in mind that what is usually called a CDW, as observed in $K_2Pt(CN)_4Br_0{\cdot}3{\times}H_2O$, blue bronze $K_{0.3}MoO_3$, or $NbSe_3$, is a $2k_F$-BOW.

Whatever the nature of the CDW state, the gain in electronic energy due to the gap opening ($E_e \sim -\Delta^2 \ln \Delta$) overcomes the loss of elastic energy due to the periodic distortion ($E_l \sim \Delta^2$). As mentioned previously, BOWs are frequent in organic compounds. In TTF-TCNQ, the most important displacements are acoustic-like,[48] and they modulate the intermolecular distances and consequently the transfer integral $t$.

It is also interesting to define the order parameter of a CDW. In the case of a BOW, the CDW and the periodic lattice distortion are in quadrature and read

$$\rho(x) = \rho_0 + \delta\rho \cos(2k_F x + \varphi) \tag{3.7}$$

$$u(x) = u_0 \sin(2k_F x + \varphi) \tag{3.8}$$

At variance for site CDWs, the modulations are in phase or out of phase with each other. Note that in general the modulations are incommensurate so that CDW has two degrees of freedom: its amplitude $\delta\rho$ and its phase $\varphi$. The order parameter is then $\delta\rho \exp i\varphi$.

The importance of the lattice in the Peierls transition leads one to define the lattice response function $\chi_u(\mathbf{q},T)$, which can be measured by X-ray scattering. Its mean-field expression is (from ref 41b, p 91)

$$\chi_u(\mathbf{q},T) = \frac{\lambda_{\mathbf{q}}}{\hbar\omega_{\mathbf{q}}} \frac{\chi_e(\mathbf{q},T)}{1 - \lambda_{\mathbf{q}}\chi_e(\mathbf{q},T)} \tag{3.9}$$

where $\lambda_{\mathbf{q}} = g_{\mathbf{q}}^2/\hbar\omega_{\mathbf{q}}$. $g_{\mathbf{q}}$ is the electron−phonon coupling, proportional to $\alpha$ (or $\beta$), and $\hbar\omega_{\mathbf{q}}$ is the energy of the phonon mode coupled to the electrons. At variance with the noncoupled case, this formula allows one to define a finite temperature $T_c^{mf}$, called the mean-field transition temperature, at which $\chi_u(\mathbf{q},T)$ diverges. More precisely, numerical calculations[24] show that above $T_c^{mf}/3$ a regime of amplitude fluctuations is observed, while below this temperature only phase fluctuations are present. $T_c^{mf}/3$ is thus close to the real phase transition temperature. (Lee, Rice, and Anderson estimated this temperature to be $T_c^{mf}/4$.[49]) Note that, in simple inorganic CDW systems, $\chi_u(\mathbf{q},T)$ can be calculated from first principles and compared to X-ray diffuse scattering measurements.[50]

Although the longitudinal value of the CDW wave vector is equal to $2k_F$, through the $\chi_e(\mathbf{q},T)$ divergence, transverse interactions are responsible for its transverse components. Three types of coupling are considered:

(1) The elastic coupling. Formula 3.9 shows that even if $\chi_e(\mathbf{q},T)$ is purely 1D, the coupling constant $\lambda_{\mathbf{q}}$ depends on the other directions. This mechanism is generally neglected.

(2) The tunneling coupling (see Figure 3a). In the presence of transverse transfer integrals, the Fermi surface is slightly warped, which determines the transverse components of the nesting wave vector. This mechanism is present in quasi-1D systems such as Bechgaard salts.

(3) The Coulomb coupling. Direct Coulomb interactions between the charged CDWs are important to consider. As shown in Figure 3b, they tend to induce out-of-phase couplings between neighboring CDWs. This mechanism is usually invoked for the CDW transverse ordering in TTF-TCNQ and related compounds.

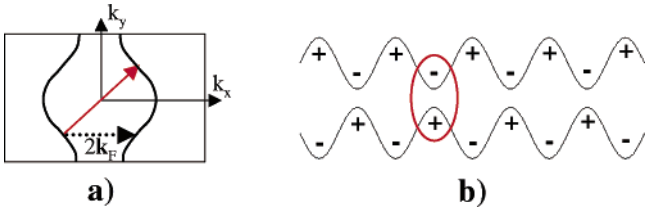


**Figure 3.** (a) Fermi surface of a quasi-1D metal. The transverse component of the nesting wave vector, indicated in red, depends on the exact shape of the Fermi surface. (b) Schematic representation of two out-of-phase CDWs. In this situation, Coulomb energy between the CDWs is minimized.

Let us now consider the effect of Coulomb interactions on 1D systems.

### 3.2.2. Electron Interactions

**Luttinger Liquid.** Many structural instabilities are triggered by the electron interactions. It is thus important to briefly describe the main results of the complex theory of the 1D electron gas. Most importantly, electron interactions change the nature of 1D instabilities. In three dimensions, a system of electrons in interaction is a *Fermi liquid*: the ground state is determined by the Fermi surface, and low-energy excitations are *quasi-particles*, which can be considered as noninteracting. In one dimension, because of the divergence of the response function $\chi_e(\mathbf{q},T)$ the Fermi liquid description in no longer valid and other theories have to be found. The first theory of the 1D electron gas was based on the *g-ology* framework in which electron interaction is described by scattering terms of amplitude $g_i$.[39] (In a 1D electron gas, two electrons on the left side (impulsion $-k_F$) or right side (impulsion $k_F$) of the Fermi surface interact with scattering terms of amplitude $g_i$. $g_1$ is the backward scattering constant, $(k_F; -k_F) \rightarrow (-k_F; k_F)$, $g_2$ is the forward scattering one, $(k_F; -k_F) \rightarrow (k_F; -k_F)$, and $g_4$ describes the $(k_F; k_F) \rightarrow (k_F; k_F)$ scattering. At half-filling, the Umklapp scattering $(k_F; k_F) \rightarrow (-k_F; -k_F)$ is possible and described by $g_3$.) The electronic dispersion $\epsilon(\mathbf{k})$ is then linearized around the Fermi energy.

The main instabilities are determined by a perturbative approach. However, this method could not deal with strong coupling. The most successful method to address this issue is the description in terms of the *Luttinger liquid*, which is now the framework of the 1D electron gas.[51−54] Indeed, for certain values of the $g_i$ constants, the interaction Hamiltonian can be solved exactly. (Two models can be solved exactly: the Tomonaga−Luttinger model, which corresponds to $g_1 = g_3 = 0$, and the Luther−Emery model, which corresponds to a special value of $g_1 < 0$.) This so-called Tomonaga−Luttinger model is the starting point of the model called a Luttinger liquid, by analogy to the 3D situation. In this model, low-energy excitations are collective spin or charge excitations. Figure 4 indicates regions where charge-density waves (CDWs), spin-density waves (SDWs), and singlet (SS) or triplet (ST) superconductivity are dominant. These regions are mainly determined by the knowledge of the relative compressibility of the electron gas $K_\rho$, which depends on the interaction

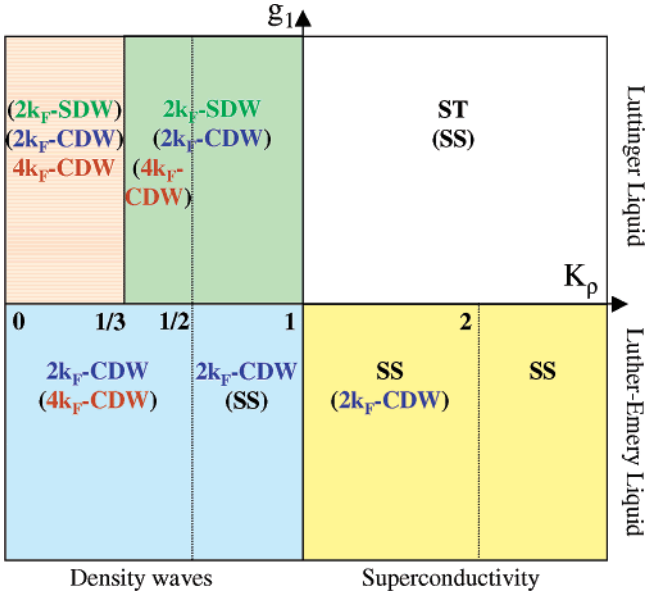


**Figure 4.** Schematic phase diagram of a correlated 1D electron gas off half-filling as a function of $K_\rho$. Dominant and subdominant (logarithmically weaker, in parentheses) instabilities are indicated. Adapted from ref 51.

constants $g_i$. $K_\rho$ decreases when the strength and the range of the interactions increase. For attracting (repulsive) interactions, one has $K_\rho \geq (\leq) 1$, with the noninteracting case corresponding to $K_\rho = 1$. For repulsive interactions, density-wave instabilities appear. Remarkably, the response functions of these instabilities are power laws (and not logarithmic ones), whose exponents depend on $K_\rho$ (see for example eqs 3.10 and 3.11). Moreover, the Luttinger liquid exhibits charge and spin separation and the absence of a Fermi edge.[54] These properties invalidate the Fermi liquid theory at one dimension.

Note that in this approach an electron (Mott) localization is observed if $K_\rho$ is smaller than a value depending on the band filling. For quarter-filling, this value is $K_\rho = {}^1/_4$, which corresponds to strongly repulsive interactions, and for half-filling, $K_\rho = 1$.[55] When the system is localized, charge excitations are frozen but the spins are still described by a Luttinger liquid.

The Luttinger liquid model is considered as relevant to describe the high-temperature phases of some organic conductors such as Bechgaard and Fabre salts, but the question is still a matter of debate.[51,56] Note that this theory does not distinguish between BOWs and CDWs, which is important to interpret experiments. Specific models such as the Hubbard model are more adapted to these situations.

One of the most important results is that electron interactions give rise to new instabilities. The $2k_F$-SDW corresponds to the modulation of the spin density at the $2k_F$ wave vector and is dominant in a region where $K_\rho \lesssim 1$. $2k_F$-SDWs are indeed observed in many molecular conductors. As the average distance between electrons is $2\pi/4k_F$ in one dimension ($\rho = 4k_F$), $4k_F$-BOW or $4k_F$-CDW instabilities naturally appear when interactions increase.[57] Note that in commensurate cases a $4k_F$-CDW corresponds to a *charge ordering* (CO), which induces a *charge disproportionation* on the molecules.

An elegant way to describe these instabilities is to express the $2k_F$ and $4k_F$ response functions as a function of $K_\rho$; one finds

$$\chi_e(2k_F,T) = N(E_F)(E_c/k_BT)^{1-K_\rho} \quad (3.10)$$

$$\chi_e(4k_F,T) = N(E_F)(E_c/k_BT)^{2-4K_\rho} \quad (3.11)$$

It is clear from these expressions that $\chi_e(4k_F,T)$ diverges if interactions are strong enough, that is, if $K_\rho \leq 1/2$, and dominates $\chi_e(2k_F,T)$ if $K_\rho \leq 1/3$. The best experimental examples are in the TTF-TCNQ series.[7,58] $4k_F$ instabilities are considered as the best evidence of electron interactions in these systems[59] and can be interpreted at least qualitatively in the framework of the Luttinger liquid.

**The Hubbard Model.** A simpler model has been developed and largely used to describe strongly correlated systems such as organic conductors: the Hubbard model.[61] In this microscopic model, the electronic Hamiltonian reads

$$H_e = \sum_{i,\sigma} t(c^\dagger_{i,\sigma}c_{i+1,\sigma} + c_{i,\sigma}c^\dagger_{i+1,\sigma}) + U\sum_i n_{i,\uparrow}n_{i,\downarrow} + \sum_{i,j} V_j n_i n_j \quad (3.12)$$

where $U$ is the on-site Coulomb energy and $V_j$ is the Coulomb energy between $j$th neighbors. (When the $V_j$ are considered, one speaks of an extended Hubbard model.) Even in this simple case, an exact solution has only been found in the $V_j = 0$ and $T = 0$ K case.[62] This solution shows that the system is metallic except in the half-filling case, where localization occurs as soon as $U \neq 0$ ($4k_F$-CDW). Numerical methods are thus necessary to study the model at nonzero temperatures or in the presence of nearest neighbor interactions.

As suggested by the exact solution, if $U$, $V \ll t$ (weak coupling), the system is metallic but develops new instabilities such as $2k_F$-SDW. In the other limit of strong coupling ($t \ll U$, $V$), the effect of interactions is to localize the electron ($4k_F$-CDW). In the half-filling case, this favors the singlet state called spin-Peierls. The three ground states $2k_F$-SDW, $4k_F$-CDW, and spin-Peierls are typical of an interacting 1D electron gas on a lattice. But they depend in a subtle way on the interactions and the band filling.

Numerous numerical simulations have been performed on the extended Hubbard model. Let us mention the work of Hirsch et al.,[57,64,65] in which the purely electronic CDW, BOW, and SDW response functions have been computed, without considering the lattice. However, as we have seen, the electron−phonon coupling can modify the results, but the results are model-dependent. Many publications present zero temperature computations taking into account the lattice, to match as closely as possible the experimental situation.[60,66−69,71−73]

### 3.2.3. Half-Filling and Spin-Peierls Phase Transition

In the half-filling case ($\rho = 1$) there is one electron per site. The effect of $U$ is to localize electrons on each site and to form a $4k_F$-CDW.[62] When the interaction $U$ is much larger than $t$, it can be shown[63] that the system is equivalent to a system of localized spins, antiferromagnetically coupled by an exchange integral $J = 4t^2/U$. The ground state is antiferromagnetic ($2k_F$-SDW). When $U$ is small and increases, the electron localization kills the divergence of the $2k_F$-CDW response function: the two states are incompatible.[64] (For a half-filled band the Umklapp term $g_3$ is responsible for the electron localization in competition with the $2k_F$-CDW instability.[82]) At variance, $V$ favors the $2k_F$-CDW at the expense of the $2k_F$-SDW. The $U = 2V$ relation separates the two ground states, which are also incompatible.[65] (Note that recent calculations on half-filled nanorings in the presence of SSH coupling indicate the possibility of CDW/SDW coexistence.[70])

When the electron−phonon coupling is considered, the $2k_F$-BOW plays a special role at half-filling. If electrons are localized by strong interactions, a $2k_F$-BOW transforms the system into an antiferromagnetic chain with alternating exchange integral $J$. In that case, the ground state is a macroscopic singlet state, with a singlet−triplet gap in the spin excitations: this is the spin-Peierls (SP) state. This name reminds us that the Peierls-like $2k_F$-BOW triggers the instability and that spin pairing plays the central role: the gain of energy is due to the decrease of the magnetic excitations across the gap. In SP phases, the singlet−triplet gap is measured by magnetic susceptibility or inelastic neutron scattering. In the "textbook" case we have described, the temperature dependence of the spin susceptibility follows the Bonner−Fisher law of a quantum $S = 1/2$ chain[74,75] and then decreases exponentially below the spin-Peierls transition. Such an example of an SP phase has been discovered in the $CuGeO_3$ oxide.[77−79] The SP states observed in organic compounds are better described by a quarter-filled approach.

### 3.2.4. Quarter-Filling and Molecular Systems

An important feature of half-filled systems is that theoretically CDW, BOW, and SDW cannot coexist.[60,69] From a general point of view,[60] the phase diagrams of quarter-filled systems are more complex because coexistence between these states is possible. Figure 5 presents some examples of such mixed ground states experimentally observed.

The connection between the extended Hubbard model and the Luttinger liquid model has been performed by Mila et al.[80] At quarter-filling the $g_i$ constants are $g_1 = U$, $g_2 = U + 2V$, $g_{4\|} = 2V$, and $g_{4\perp} = U + 2V$. Numerical calculations show that in a ($U$, $V$) domain such that $V < 2t$ the compressibility coefficient verifies $0.25 < K_\rho < 0.9$. From the diagram of Figure 4, the $2k_F$-CDW, $4k_F$-BOW, and $2k_F$-SDW instabilities are expected in this domain.

To describe all the ground states observed in molecular conductors, a quarter-filled approach is more consistent. However, the spin-Peierls transition, typical of half-filling systems, is stabilized in some of these systems. This SP state is observed when electrons are localized either in a $4k_F$-BOW or in a mixed $4k_F$-BOW/CDW. The first situation is found in the TTF-CuBDT[74,83] compounds (in which the SP

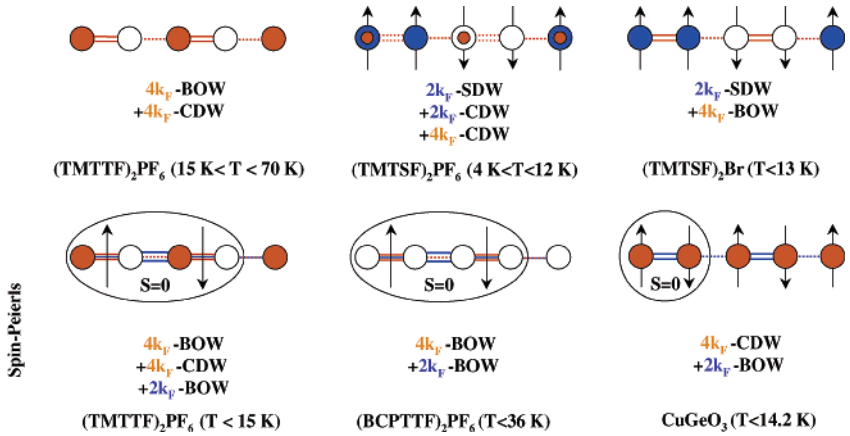


**Figure 5.** Schematic representations of some mixed ground states. Open (colored) circles represent the minima (maxima) of the site CDW, and dashed (double) lines represent the minima (maxima) of the BOW. Blue (orange) is for $2k_F$ ($4k_F$) modulations. The second row represents spin-Peierls states observed in quarter-filled organic systems and in the half-filled oxide $CuGeO_3$, for comparison.

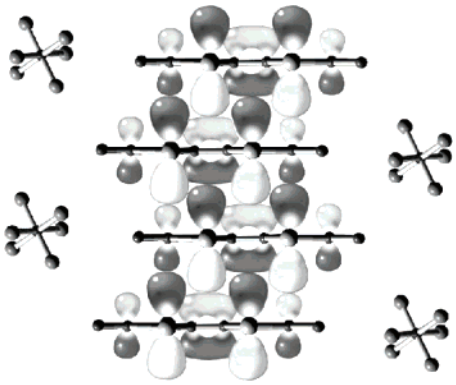

**Figure 6.** Side view of $(TMTTF)_2PF_6$. The $a$ axis is vertical. (Courtesy of Jean-Jacques Riquier.)

transition was discovered), MEM-TCNQ[84,85] and the $(BCPTTF)_2X$.[141,142] Fabre salts $(TMTTF)_2PF_6$,$AsF_6$ correspond to the second class,[87−89] which will be discussed later.

We will also show that $2k_F$-BOW fluctuations can transform into spin-Peierls ones,[160] showing that the two types of fluctuations can be described by the same physics.

## 4. Experimental Results: Structural Instabilities

### 4.1. The $(TM)_2X$ Series

Given the number of papers devoted to the study of Bechgaard and Fabre salts (which will be noted $(TM)_2X$ for simplicity), these materials can be considered as the prototype of quasi-1D organic systems.[34,56] In this section, we will present some new structural properties which have been obtained in the past few years. However, more details will be found in ref 8.

#### 4.1.1. Basic Structure of Bechgaard and Fabre Salts

$(TM)_2X$ salts are all isostructural. The space group is $P\bar{1}$.[92] Molecules stack in the **a** direction ($a \sim 7.5$ Å) (see Figure 6) and form conducting chains. The chains regroup in (**a**, **b**) slabs separated by anions in the **b** direction. The highest conductivity is observed in the **a** direction (500−800 $(\Omega\ cm)^{-1}$ in selenied salts, 50−100 $(\Omega\ cm)^{-1}$ in sulfur salts). In this direction the molecules are related by an inversion center and anions are located in centrosymmetric cavities. A three-quarter-filled band is expected from the 2:1 stoichiometry, but the real band filling is formally half, because the unit cell contains two molecules.

Contrary to charge-transfer salts such as TTF-TCNQ, $(TM)_2X$ salts are slightly dimerized. This dimerization is weak but important, because it corresponds to a $4k_F$-BOW which can localize electrons.[73,90,91] This dimerization is usually characterized by $2(d_1 - d_2)/a$, where $d_1$ and $d_2$ are the average distances between molecules along the chains ($2(d_1 - d_2)/a \sim 0.8\%$ for $(TMTTF)_2X$ for example). However, the parameter which affects the electronic properties is the difference between transfer integrals along the chain.[8] Indeed, it contributes with the external anion potential to the zone boundary gap at $\pm\pi/a$.[8]

These integrals have been calculated in the extended Hückel framework.[93,94] With this definition of the dimerization, it is found that it is larger in the TMTTF salts than in the TMTSF ones, that it *decreases* when the lattice contracts (at low temperature or high pressure), and that it depends on the anion X (it decreases according to the sequence $PF_6 \rightarrow ClO_4$, $ReO_4 \rightarrow NO_3$, Br). This structural dimerization seems to be due to the steric constraint given by anions.[8]

The geometry of the X anions can be spherical (Br), octahedral ($PF_6$, $AsF_6$, $SbF_6$), tetrahedral ($ClO_4$, $BF_4$, $ReO_4$), triangular ($NO_3$), or linear (SCN). A specificity of the $(TM)_2X$ salts is that nonsymmetrical anions are always disordered at room temperature[8] and that they undergo order−disorder phase transitions. This is not the case for all 2:1 charge-transfer salts.

#### 4.1.2. Phase Diagram

A generalized pressure−temperature phase diagram of the $(TM)_2X$ series has been proposed,[56] where the main salts of the series find a place according to their ambient pressure ground state. New results on $(TMTTF)_2PF_6$[32,33] confirmed that all the main ground states of the salts can be found in the same compound. Such a diagram is presented in Figure 8. On

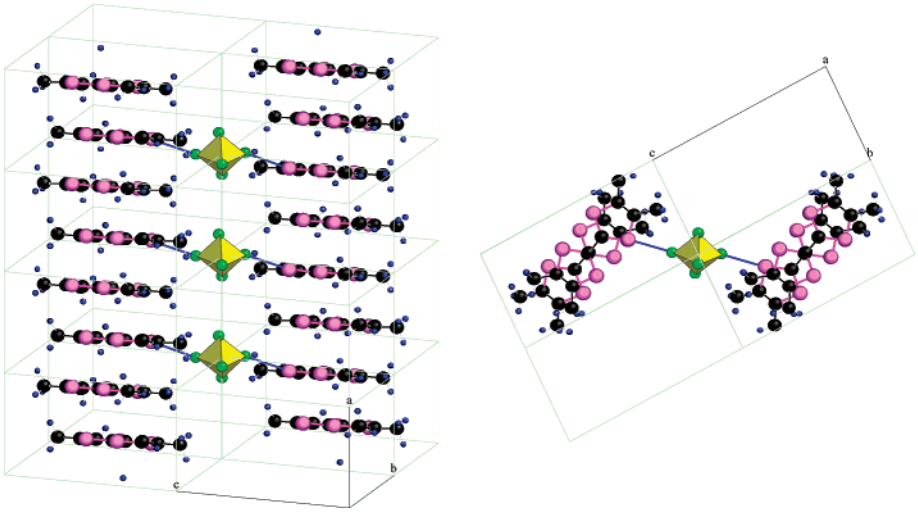

**Figure 7.** Schematic representation of the anions and their environment in $(TMTTF)_2PF_6$. Short F−S contacts are indicated.

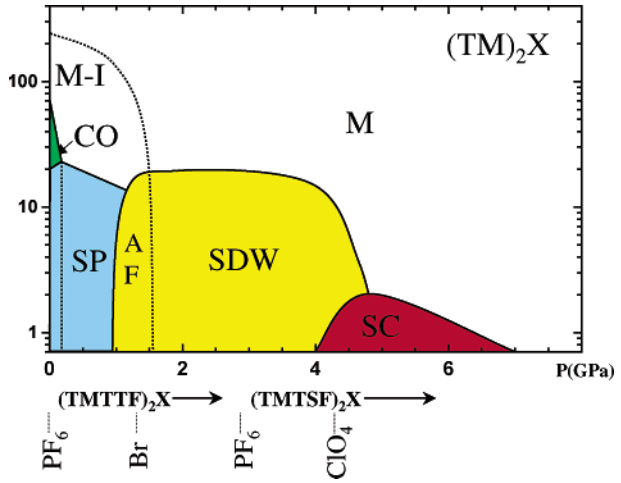


**Figure 8.** Generalized phase diagram $(T, p)$ of the $(TM)_2X$ salts. M−I is the Mott−Hubbard localized state, M the metallic phase, SC the superconducting phase, AF the antiferromagnetic phase, and CO the charge ordering phase. The pressure values correspond to the $(TMTTF)_2PF_6$ phase diagram,[33] except for the CO domain, which has been inferred from the $(TMTTF)_2AsF_6$ data of ref 95.

the left side, electronic localization occurs at ~200 K, then CO is observed and the SP transition is stabilized below 18 K. At higher pressure, a localized antiferromagnetism appears and a $2k_F$-SDW is stabilized. Finally, between 4 and 7 GPa, $(TMTTF)_2PF_6$ exhibits superconductivity. According to ref 56, the high temperature−low pressure part of the diagram is correctly described by a Luttinger liquid while at higher pressure a Fermi liquid picture is more appropriate.

Indeed, this phase diagram, together with the theoretical considerations mentioned previously, makes it clear that electronic interactions are crucial in the understanding of the physical properties of $(TM)_2X$. From optical reflectivity measurements,[81] Mila[80] estimated the basic parameters $t_2/t_1$, $U/t_1$, and $V/t_1$ of the extended Hubbard model in two important compounds (see Table 1). These results, compared to the numerical computations of ref 66, give $K_\rho \sim 0.45$ for $(TMTSF)_2ClO_4$ and $K_\rho \sim 0.3$ for $(TMTTF)_2PF_6$. According to the general results of Figure 4, these compounds would be in a region where $2k_F$-SDWs, $2k_F$-CDWs, and $4k_F$-CDWs are in competition, which is consistent with the experimental results (see section 4.1.6). Note, however, that another estimation gives $K_\rho \sim 0.22-0.23$ for $(TMTSF)_2PF_6$.[56]

**Table 1. Estimation of the Basic Parameters $t_2/t_1$, $U/t_1$, and $V/t_1$ of the Extended Hubbard Model in the $(TMTSF)_2ClO_4$ and $(TMTTF)_2PF_6$ Compounds (Data from ref 80)**

| | $t_2/t_1$ | $U/t_1$ | $V/t_1$ |
|---|---|---|---|
| $(TMTSF)_2ClO_4$ | 0.9 | 5.0 | 2.0 |
| $(TMTTF)_2PF_6$ | 0.7 | 7.0 | 2.8 |

Finally, note that this phase diagram does not take into account the anions. Moreover, the recent observation of ferroelectricity (FE) and anti-ferroelectricity (AFE)[100−102] makes this phase diagram more complex, as discussed in the next sections.

### 4.1.3. Structural Instabilities

Some members of the $(TM)_2X$ family exhibit typical 1D structural instabilities. In $(TMTSF)_2PF_6$ and $AsF_6$, diffuse lines at the $2k_F = \pi/a$ reduced wave vector have been observed by X-ray measurements,[96] below 150−175 K (see Figure 9). Such lines are clear signatures of a $2k_F$-BOW because they are visible at wide angles. [BOWs, which are displacement modulations, give rise to wide angle diffuse scattering (eq 2.12), while pure CDWs contribute to small angles, because they modulate the electron density (eq 2.11).] From this point of view, these fluctuations are similar to the ones observed in TMTSF-TCNQ,[97] but they do not diverge toward an ordered $2k_F$-BOW ground state. Indeed, the widths of the diffuse lines give maximum correlation lengths of ~10 Å, and their intensity decreases below 50 K. This corresponds to the temperature at which 2D or 3D SDW fluctuations observed by NMR[98] build up. This does not mean that the $2k_F$ instabilities vanish, because $2k_F$-CDW satellite reflections have been observed at lower temperature, in the SDW phase, as we will describe in section 4.1.6.

At first sight, the behavior of $(TMTTF)_2PF_6$ seems different. A charge localization is first observed at $T_\rho \sim 200$ K[88] with a charge gap $\Delta_\rho \sim 600$ K.[88,104] This localization is not associated with a phase transition

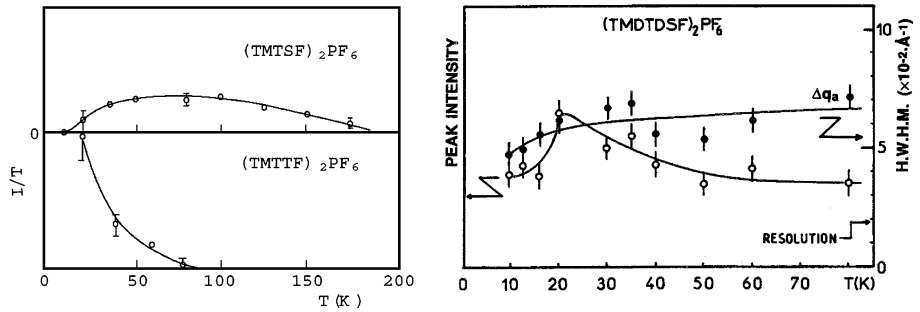


**Figure 9.** Temperature dependence of the intensity (open circles) and the hwhm (closed circle) of the $2k_F$ diffuse lines in $(TMDTDSF)_2PF_6$ (top) and of the $2k_F$ response function $\sim I/T$ in $(TMTSF)_2PF_6$ and $(TMTTF)_2PF_6$ (bottom).

and is usually interpreted as a $4k_F$-BOW, which has the periodicity of the main lattice. Below 70 K, diffuse lines at the $2k_F = \pi/a$ reduced wave vector are observed,[87] indicating the presence of $2k_F$-BOW fluctuations. These fluctuations diverge at $T_{SP} = 18$ K, as indicated by the presence of satellite reflections at the ($1/2$, $1/2$, $1/2$) reduced wave vector below $T_{SP}$. This phase has been impossible to study by X-ray diffraction because of irradiation damage,[87] but it has been recently shown by neutron scattering that these satellite reflections condense below $T_{SP}$, indicating definitely that it is a SP transition.[99] The observation of $2k_F$-BOW diffuse lines clearly demonstrates the 1D character of the electron gas in TMTTF salts.

An intermediate behavior has been observed in $(TMDTDSF)_2PF_6$ in which $2k_F$ diffuse lines (see Figure 9 and section 5.3.1) are observed from 150 K down to 20 K. Below this temperature $2k_F$-SDW fluctuations begin to diverge,[153] and the intensity of the lines decreases by a factor of 2. The 3D ordering of $2k_F$-SDWs is not achieved, however, probably because of the molecular disorder. This shows that there is a continuity between the 1D instabilities of $(TMTSF)_2PF_6$ and $(TMTTF)_2PF_6$. The $2k_F$-BOW fluctuations of $(TMDTDSF)_2PF_6$ have a mixed CDW−SP character.

These observations show that although the $2k_F$-BOW instability is present in the $(TM)_2X$ family, it can only give rise to the SP ground state. Indeed, in the metallic part of the $(TM)_2X$ diagram it is killed by 3D $2k_F$-SDW fluctuations, while in the left part of the phase diagram it is in competition with another newly discovered instability, the $4k_F$-CDW charge ordering. This is consistent with the study of (TMTSF/TMTTF) solid solutions (see section 5.3.3) and substituted perylene salts (see section 5.2), in which the occurrence of a $4k_F$-CDW clearly suppresses the $2k_F$-BOW divergence.

### *4.1.4. Charge Ordering Transitions*

The discovery of CO transitions in Fabre salts has been one of the most surprising results of the past few years. In 1984, a metal−insulator phase transition was observed at 154 K in $(TMTTF)_2SbF_6$, without any observable structural change.[104] These so-called "structureless" transitions were recently discovered in $(TMTTF)_2PF_6$, $AsF_6$, and $ReO_4$, at 70, 100, and 225 K, respectively, and recognized to correspond to FE.[100] Indeed, dielectric permittivity[100] and NMR measurements[101] in $(TMTTF)_2PF_6$, $AsF_6$, $SbF_6$, and $(TMTTF)_2ReO_4$, SCN compounds,[103] lead to the conclusion that these FE ($\mathbf{q} = 0$) and AFE ($\mathbf{q} \neq 0$) states (in $(TMTTF)_2SCN$) are associated with a charge ordering (CO) and result from the loss of the symmetry center relating the molecules of the chain. CO gives rise to small though visible anomalies on resistivity curves.[104,100] The CO can be interpreted as the stabilization of $4k_F$-CDWs either in phase in all the transverse directions (FE case) or out of phase in some transverse directions (AFE case).

However, even if internal deformations of the molecules are expected, diffraction[105] and absorption methods[106] have failed to evidence structural modulations associated with the FE CO transition.[105] Such deformations have been clearly measured in $(TMTTF)_2SCN$,[107] where the AFE CO phase corresponds to the appearance of (0, $1/2$, $1/2$) satellite reflections. In that case, the charge disproportionation resulting from the CO was found to be $\Delta\rho = 0.15$ (half the difference between the charge of the two molecules). Transfer integral dimerization decreases at the transition, indicating the competing character of the $4k_F$-CDW and $4k_F$-BOW order parameter, which is in agreement with the numerical calculation of ref 72.

In substituted perylene salts $(TMP)_2X-S$ ($X = PF_6$, $AsF_6$)[108,109] (see section 5.2), a $4k_F$-CDW was clearly evidenced by a combination of X-ray and $^{13}C$ NMR techniques. This $4k_F$-CDW corresponds to the same type of CO discussed here. More recently, CO transitions have been observed in other salts, like (DI-DCNQI)$_2$Ag,[110] $\theta$-$ET_2MM'(SCN)_4$,[111,112] α-$(BEDTTTF)_2I_3$,[114,113] and $\beta$-$(BEDTTTF)_2AsF_6$ and $PF_6$.[115] Note that the surprising alternation of TMTSF and TMTTF molecules found in the solid solutions $(TMTSF)_{1-x}(TMTTF)_xReO_4$[116] can also be considered as a charge ordered $4k_F$-CDW. This will be discussed in section 5.3.3.

To conclude this section, let us note that in 2:1 charge-transfer salts the difficulty of finding $\mathbf{q} = 0$ CO or more generally $4k_F$-CDWs or $4k_F$-BOWs by structural methods comes from the triclinic symmetry of most salts: the CO ($4k_F$-CDW) only breaks the inversion center (and leads to a real phase transition), while the dimerization ($4k_F$-BOW) does not break any symmetry. In this respect the best evidence of charge ordering has been brought by NMR measurements[95,101,109,111,114] (and see section 5.2). Overcoming this difficulty is not trivial because it requires the synthesis of more symmetrical salts, such that $4k_F$-CDWs or $4k_F$-BOWs break another symmetry element. To our knowledge, only two 2:1

**Table 2. Reduced Wave Vector $\mathbf{q}_{AO}$ and Transition Temperature $T_{AO}$ of the Anion Ordering Transitions Observed in the $(TM)_2X$ Compounds for Various Anions**

| | $(TMTSF)_2X$ | | $(TMDTDSF)_2X$[160] | | $(TMTTF)_2X$ | |
|---|---|---|---|---|---|---|
| X | $T_{AO}$/K | $\mathbf{q}_{AO}$ | $T_{AO}$/K | $\mathbf{q}_{AO}$ | $T_{AO}$/K | $\mathbf{q}_{AO}$ |
| $ReO_4$ | 176 | $(1/2, 1/2, 1/2)$[86] | 165 | $(1/2, 1/2, 1/2)$ | 154 | $(1/2, 1/2, 1/2)$[119] |
| | 240 (17 kbar) | $(0, 1/2, 1/2)$[154] | | | | |
| $BF_4$ | 36 | $(1/2, 1/2, 1/2)$[118] | 22 | $(1/2, 1/2, 1/2)$ | 40 | $(1/2, 1/2, 1/2)$[121] |
| | | | quasi-phase transition | | | |
| $ClO_4$ | 24 | $(0, 1/2, 0)$[120] | local order | $(1/2, 1/2, 1/2)$ | 40 | $(1/2, 1/2, 1/2)$[87] |
| $NO_3$ | 41 | $(1/2, 0, 0)$[86] | local order | $(1/2, 0, 0)$ | 50 | $(1/2, 0, 0)$[121] |
| SCN | 90 | $(0.48, \overline{0.35}, 0.1)$[122] | | | 160 | $(0, 1/2, 1/2)$[124] |
| $FSO_3$ | 87.5 | $(1/2, 1/2, 1/2)$[121] | | | 58 | not known |
| $PF_2O_2$ | 136.3 | $(1/2, \pm 1/4, 0)$ | | | | |
| | 135.3 | $(0, 1/2, 1/2)$[123] | | | | |

charge-transfer salts satisfy such a requirement: (i) $(EDT\text{-}TTF{-}CONMe_2)_2AsF_6$,[117] in which a glide plane ensures the uniform stacking, and (ii) the monoclinic form of the $(DMtTTF)_2X$ series, obtained with X = $ReO_4$ and $ClO_4$,[12] in which a $2_1$ screw axis plays this role. The former compound is localized at ambient temperature, while the later ones exhibit a charge localization at about 150 K. Consequently, such compounds with uniform stacks are *really* quarter-filled, even though the real periodicity of the chain is still twice the intermolecular distance. Let us insist on the fact that in such cases any kind of electronic localization coupled to the lattice should break this "quarter-filled symmetry". Indeed, a charge disproportionation would make the sites (molecules) inequivalent, while a dimerization will unsymmetrize the bonds. Contrary to this expectation, however, it has been shown that $(DMtTTF)_2ClO_4$ exhibits a complex incommensurate short-range order modulation below the charge localization, which has been interpreted as AFE in nature.[106]

A simple extrapolation of the CO domain phase boundaries of the diagram in Figure 8 shows that in the "negative" pressure range this phase should dominate the SP state ($2k_F$-BOW) and the electron localization ($4k_F$-BOW). In this respect, it is interesting to note that in compounds with large anions such as $SbF_6$ and $ReO_4$, which could induce such a "negative" pressure, the CO transitions are observed at *higher* temperature than those of the AF state and the $(1/2, 1/2, 1/2)$ AO, respectively. Finally, it has been suggested that the CO transition should be coupled to anionic displacements,[73,102] the same way the orientation of non-centrosymmetrical anions is coupled to electronic degrees of freedom. This is the subject of the next section.

### *4.1.5. Role of Anions*

In $(TM)_2X$ salts, anions play an important role to ensure the charge transfer but also because they induce a $4k_F$ potential along the chains of molecules.[90,91] This is clearly seen in Figure 7, where the $PF_6$ anions and their nearest neighboring molecules are represented. In particular, the F atoms of the $PF_6$ anions (or the O atoms of $ReO_4$) have close contacts with the S (or Se) atoms of the molecules. Depending on the stength of this potential, numerical calculations show that $4k_F$-BOWs or $4k_F$-CDWs can be stabilized.[73] Both instabilities have now been observed in the $(TM)_2X$ salts. The role of this $4k_F$ potential on the $2k_F$-BOW instability has also been questionned.[82] Note that the study of the CO transition and the solid solution (TMTSF/TMTTF) clearly shows that the $4k_F$-CDW decreases the $2k_F$-BOW response function.[73]

Structural studies show that non-centrosymmetrical anions can have two orientations in the unit cell and are disordered at high temperature. Anion ordering phase transitions are observed, with a reduced wave vector which depends on the anion and the molecule.[8] Some characteristics of anion ordering transitions are indicated in Table 2.

Some of these phase transitions are strongly coupled to the electronic degrees of freedom and have a drastic influence on the physical properties. The AO at 176 K in $(TMTSF)_2ReO_4$ correponds to a metal−insulator transition.[86] This transition stabilizes the $(1/2, 1/2, 1/2)$ wave vector, which means that the anion orientations alternate in the three directions of the unit cell. It can be considered as a generalized Peierls transition, because the component of the wave vector along the chain (**a** direction) corresponds to $2k_F$. Under pressure, the metallic state is recovered and another AO at the reduced wave vector $(0, 1/2, 1/2)$ is observed.[154] The electronic degrees of freedom are slightly affected by this AO, which confirms the importance of the $2k_F$ component. However, the stabilization of an $(1/2, 1/2, 1/2)$ AO is not sufficient to induce an insulating state: this is the case of $(TMTSF)_2NO_3$. This clearly shows that the strength of the anion−donor coupling is another relevant parameter of AO.

The study of AO transitions has shown that the driving forces of these transitions are both direct (mainly electrostatic) and mediated by the electron gas of the organic chains. More details can be found in ref 8. Finally, note that such transitions can be easily modeled by an Ising model, already introduced in section 2.4. This modeling will be used in section 5.

### *4.1.6. Mixed States BOW–CDW–SDW*

As shown previously, the phase diagram $(TM)_2X$ has turned out to be more complicated than first believed. In particular, the discovery of CO transitions in the S-based salts has shown that the ground states are in fact *mixed* states, in which different possible order parameters of the 1D theory are

stabilized simultaneously. Such mixed states are also observed by X-ray diffraction in the TMTSF series, which confirms these conclusions.

In $(TMTSF)_2PF_6$, the metal−insulator phase transition observed at $T_{SDW} = 12$ K corresponds to a $2k_F$-SDW state, as evidenced by spin susceptibility anisotropy,[125] observation of antiferromagnetic resonance,[126] and NMR and Muon Spin Resonance ($\mu$SR) measurements.[127] Direct determination of the magnetic wave vector $\mathbf{q}_{SDW}$ has failed, mainly because of the small size of the samples. However, it has been possible by NMR experiments to estimate that the reduced wave vector is $\mathbf{q}_{SDW} = (0.5, 0.20 \pm 0.05, ?)$[129] or $(0.5, 0.24 \pm 0.03, -0.06 \pm 0.20)$.[130]

The X-ray studies of these SDW phases are described in detail in ref 8. Let us just summarize here the results.

(1) In $(TMTSF)_2PF_6$, satellite reflections at the reduced wave vector $\mathbf{q}_1 = (0.5 \pm 0.05, 0.25 \pm 0.05, 0.25 \pm 0.05)$ and $\mathbf{q}_2 = 2\mathbf{q}_1$ have been observed in the SDW state. These observations have been confirmed by Kagoshima et al.,[137] who show furthermore that the reflections disappear below 3.2 K. Such satellite reflections were also observed in $(TMTSF)_2AsF_6$.[137] In $(TMTSF)_2Br$, satellite reflections on the $h$ = odd main Bragg layer are observed in the AF state.[8]

(2) The location of the satellite reflections does not correspond to the $2k_F$-BOW diffuse lines already mentioned. Their intensity is very weak ($\sim 10^{-5}$ of the $(10\bar{1})$ reflection). They are observed at small angles (except for $(TMTSF)_2Br$). The features suggest that the origin of these reflections is pure CDWs. The ground state of $(TMTSF)_2PF_6$ would be a mixed state $4k_F$-CDW/$2k_F$-CDW/$2k_F$-SDW, as depicted in Figure 5. From the satellite reflection intensities, the amplitude of the CDW can be estimated to be 0.1 e,[128,133] which is consistent with the SDW amplitude of 0.08 $\mu_B$ obtained by NMR. For $(TMTSF)_2Br$, a $4k_F$-BOW/$2k_F$-SDW mixed state is consistent with the observations, which is similar to the situation observed in chromium.[134]

Such mixed states could be a clue to understand the discrepancies with the standard SDW theory, like the weak first-order character of the transition[127,131] or the effective mass enhancement of the SDW.[41a] More recently, a similar $2k_F$-CDW/$2k_F$-SDW mixed state has been suggested in α-$(BEDT\text{-}TTF)_2MHg(SCN)_4$ (M = K, Rb).[136]

From a theoretical point of view, let us mention first that Overhauser[135] had already predicted $2k_F$-CDW/$2k_F$-SDW mixed states, that he described phenomenologically by the superposition of two $2k_F$-CDWs of opposite spins.[8] Many theoretical works have been devoted to the mixed state.[60,69,138−140] All these works show that only quarter-filled models with second neighbor $V_i$ electron interactions can account for mixed states, even though no mean-field solution has been found to stabilize a $4k_F$-CDW/$2k_F$-CDW/$2k_F$-SDW state. Finally, Mazumdar et al. pointed out that transverse interactions allow us to account for complex mixed states, that he denoted BCSDW for bond-charge-spin-density waves. These mixed states are nevertheless far from being understood.

## 4.2. Spin-Peierls Transition in $(BCPTTF)_2X$

As mentioned previously, irradiation damage made the study of the SP transition in TMTTF salts impossible. To overcome this difficulty, the SP state was studied in the $(BCPTTF)_2X$ series, in which such effects were never observed.[141,142]

BCPTTF (benzocyclopentyltetrathiafulvalenium) is a non-centrosymmetric molecule (see Figure 1),[94] which gives 2:1 salts with $PF_6$ and $AsF_6$, isostructural to the $(TM)_2X$ ones. In $(BCPTTF)_2X$, charges are more localized ($\Delta_\rho \sim 1000$ K[94]) than in TMTTF salts, probably due to a $4k_F$-BOW. (The best evidence for $4k_F$-CDWs is given by dielectric susceptibility and NMR measurements, which have not been performed on all molecular conductors so far.) The magnetic susceptibility $\chi_s$ exhibits above 100 K a Bonner−Fisher thermal dependence expected for a 1D quantum $S = {}^1/_2$ AF chain (Figure 8). Below $T_{SP} = 36$ K (32.5 K), a SP state is stabilized in $(BCPTTF)_2PF_6$ ($AsF_6$), as evidenced by a strong decrease of $\chi_s$ together with the appearance of satellite reflections at the $({}^1/_2, {}^1/_2, {}^1/_2)$ wave vector.[142] $2k_F$ diffuse scattering is observed up to $T_0 = 100$ K (120 K) in the $PF_6$ ($AsF_6$) salt, indicating a strong regime of pretransitional fluctuations. At this temperature, the correlation length along the chains is found to be equal to the $a$ parameter, that is, the distance between spins. The behavior of these 1D fluctuations is indicated in Figure 10.

The most important result is that $\chi_{sp}$ starts to deviate from the Bonner−Fisher value at the temperature $T_0$, that is at the temperature at which critical fluctuations start to pair neighboring spins. This mechanism has been checked by theoretical calculations by Dumoulin et al.[159] by a microscopic treatment of the spin-phonon coupling, combining functional integral and transfer matrix methods.

It is noteworthy that these conclusions are only correct because the $(BCPTTF)_2X$ compounds are in the adiabatic limit. In this limit, the spin excitations are faster than the lattice vibrations, so that the spins can follow the lattice. To be more quantitative, Schulz[143] showed that the relevant parameters to compare are the bare frequency of the phonon mode $\Omega_0$ and the mean-field temperature of the SP transition $T_F$. In our case, this temperature is roughly equal to the temperature at which structural fluctuations build up. The ratio $T_F/\Omega_0 \geq 1$ corresponds to the adiabatic limit, where a soft mode is expected, while $T_F/\Omega_0 \leq 1$ corresponds to the nonadiabatic limit. In $(BCPTTF)_2X$, $\Omega_0 \sim 60$ K, which gives $T_F/\Omega_0 \sim 2$ and confirms the adiabatic situation. Note that in intermediate cases, $T_F/\Omega_0 \sim 1$, hardening of the phonon modes is expected, which has been observed in the inorganic $CuGeO_3$ compounds.[145]

To confirm this analysis, dynamic studies would be needed. However, in organic compounds, inelastic neutron scattering measurements are difficult to perform because of the small size of crystals.

## 4.3. Charge-Density Waves in $M(dmit)_2$ Compounds

The observation of a metallic state in molecular materials pushed chemists to synthesize new precur-

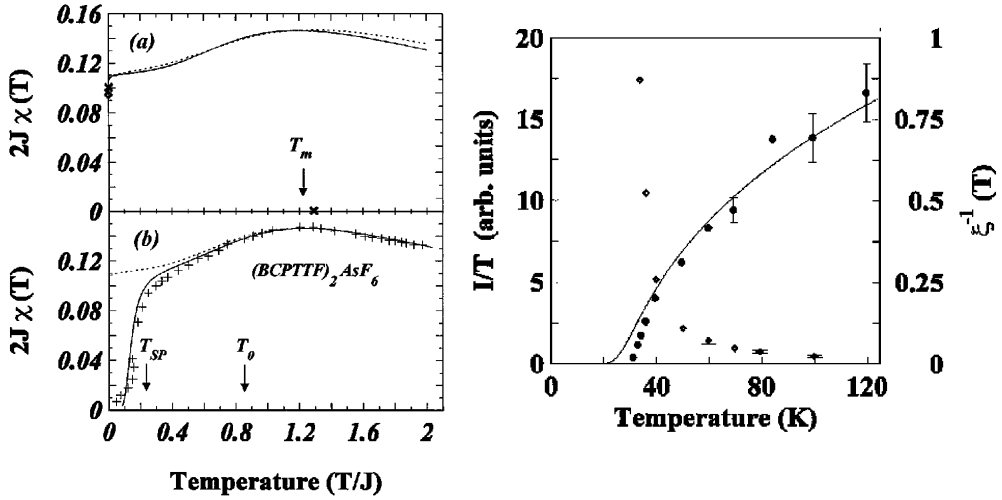


**Figure 10.** Magnetic susceptibility as a function of temperature (left): top, calculations of ref 142 (straight curve) and of ref 76 (dotted line); bottom, experimental points from $(BCPTTF)_2AsF_6$, together with calculations with (solid curve) and without lattice fluctuations (dotted curve). Here, $J = 140$ K and $T_0 \sim 120$ K. Right: $2k_F$ response function $\sim I/T$ and reduced correlation length along the spin chains $a/\xi$.

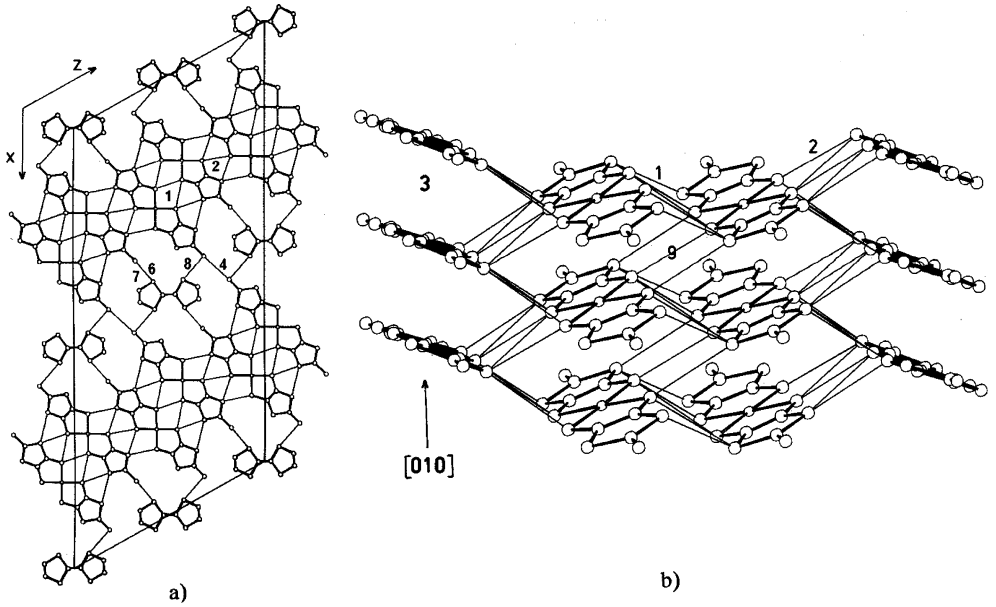


**Figure 11.** Crystal structure of $TTF[Ni(dmit)_2]_2$: (a) projection onto the (010) planes; (b) parallel view along [010] of the $Ni(dmit)_2$ slabs.

sors. We already mentioned some criteria to obtain "good" molecules. In this respect, the study of TM and BEDTTTF salts has clearly indicated that strong lateral S−S or Se−Se interactions could hinder the appearance of 1D instabilities.

Increasing the number of S atoms around the molecule was the strategy used by Cassoux et al. to synthesize materials based on the $[M(dmit)_2]^{n-}$ (refs 146 and 147) complex, where dmit is dimercaptoisodithione and M is a metallic atom like Ni, Pd, or Pt (see Figure 1). These acceptors form different phases with donors such as TTF,[147,148] $NMe_4$,[149] or Cs.[150] Among these phases, $TTF[Ni(dmit)_2]_2$ is metallic at ambient pressure and a superconductor at 1.6 K under 7 kbar.[35] The isostructural salt α′-$TTF[Pd(dmit)_2]_2$ exhibits metallic behavior at room temperature and an activated conductivity below 220 K. Under 20 kbar, this insulating phase disappears and superconductivity is stabilized below 6 K.[151] These phases consist of segregated stacks of TTF and $M(dmit)_2$ molecules, running in the **b** directions (see Figure 11). The $M(dmit)_2$ molecules are regrouped in (**b**,**c**) slabs, in which close S−S contacts are observed. However, despite the 2D characteristics, these compounds exhibit typical 1D ground states.

Figure 12 displays a X-ray precession photograph of the (*hk*0) reciprocal at room temperature obtained on the α′-$TTF[Pd(dmit)_2]_2$ compound. Diffuse lines (corresponding to diffuse sheets in the reciprocal space) at the reduced wave vectors $\mathbf{q}_1 = 0.5\mathbf{b}^*$ and $\mathbf{q}_2 = \pm 0.31\mathbf{b}^*$ are clearly visible. This diffuse scattering is characteristic of 1D CDW instabilities. In fact, two phase transitions are observed in this compound. The first one, at $T_1 = 150 \pm 10$ K, corresponds to the condensation of the diffuse scattering in satellite reflections at the reduced wave vector (0, 0.5, 0), and the second one, occurring at $T_2 = 105 \pm 10$ K, corresponds to (0, ±0.31, 0) satellite reflections. Note, however, that long-range order is never observed, because the width of the satellite

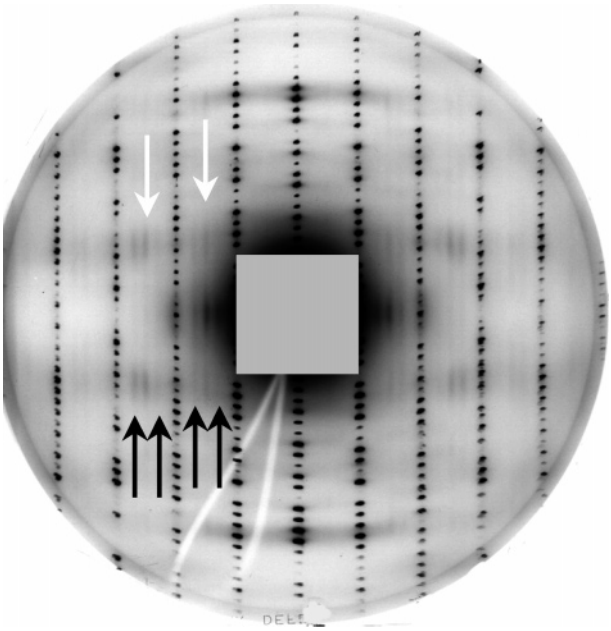

**Figure 12.** X-ray precession photograph of the ($hk$0) reciprocal at room temperature obtained on the α′-TTF-[Ni(dmit)$_2$]$_2$ compound. The chain direction **b** is horizontal. White arrows indicate the diffuse sheet located at $\mathbf{q}_1 = 0.5\mathbf{b}^*$, and black arrows indicate the diffuse sheets located at $\mathbf{q}_2 = \pm 0.31\mathbf{b}^*$.

reflections is larger than the experimental resolution. This unusual situation is all the more complex because two other types of broad satellite reflections are observed at lower temperature (25 K), located at $2\mathbf{q}_2 = \pm 0.62\mathbf{b}^*$ and $\mathbf{q}_1 - \mathbf{q}_2 = 0.81\mathbf{b}^*$. In the TTF-[Ni(dmit)$_2$]$_2$ compound, the situation is simpler: only one series of diffuse sheets at $\pm 0.40\mathbf{b}^*$ is observed from 300 K down to 40 K, the temperature at which 3D correlations build up. Here also, long-range order is not stabilized.

These complex behaviors are impossible to understand by comparison to the TTF-TCNQ componds, in which "only" $2k_F$- and $4k_F$-BOWs were observed. The solution came from the band structure calculation of Canadell et al.,[156,157] using the extended Hückel method to model molecular orbitals. The key to understand the electronic structure is to note that the energy difference between HOMOs and LUMOs of M(dmit)$_2$ molecules (0.4 eV) is smaller than that in other organic molecules. Because of the good overlap between orbitals along the chains, the electronic dispersion along the chains is larger than this energy. The band structure of the Pd(dmit)$_2$ slabs of α′-TTF[Pd(dmit)$_2$]$_2$ is indicated in Figure 13.

This unique situation means that HOMOs of M(dmit)$_2$ can give electrons, which is unusual for an acceptor. Note, however, that the determination of the Fermi level is not possible from this calculation. The experimental reduced wave vectors $\mathbf{Q}_1 = \mathbf{q}_1/2$ and $\mathbf{Q}_2 = \mathbf{q}_2/2$ are indicated in Figure 13. Given the uncertainties concerning the charge transfer, two interpretations of the wave vector values can be given:

(1) The four LUMO bands are nested by $\mathbf{q}_1$, and the upper pairs of the HOMO bands are nested by $\mathbf{q}_2$. The HOMO's lower pair would be nested by $\mathbf{q}_1 - \mathbf{q}_2$. Charge conservation thus implies a charge transfer of $\rho = 1$, which allows $\mathbf{q}_1$ to nest the TTF band. [Denoting $k_F^L$, $k_F^H$, and $k_F^T$ the Fermi wave vectors of the Pd(dmit)$_2$ LUMOs, HOMOs, and TTF bands, respectively, charge conservation gives $4(4k_F^L) + 4(4k_F^H) + 2(4k_F^T) = 8$, because eight holes come from four LUMOs.]

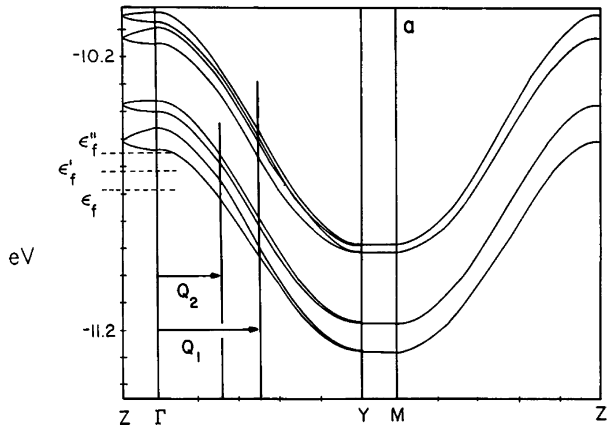


**Figure 13.** Band structure of Pd(dmit)$_2$ in α′-TTF[Pd-(dmit)$_2$]$_2$. The Γ, Y, Z, and M points are (0, 0), (b*/2, 0), (0, c*/2), and (0, c*/2). The four upper bands are built from LUMOs of Pd(dmit)$_2$ molecules, and the four lower bands are from HOMOs. The Fermi levels noted $\epsilon_f$, $\epsilon'_f$, and $\epsilon''_f$ correspond to charge transfers of 0, 1/2, and 1, respectively. Note that TTF bands are not represented here (reprinted with permission from ref 156, copyright 1989 EDP Sciences).

(2) The four LUMO bands are nested by $\mathbf{q}_1$, and the four HOMO bands are nested by $\mathbf{q}_2$. $2\mathbf{q}_1$ would then nest the TTF band. The charge transfer would be $\rho = 0.76$, which is closer to the values observed in other TTF compounds.[7]

Both solutions are in agreement with the calculation within 0.05 eV errors. They show how to remove all electrons from the Fermi surface with only two modulations. These calculations also allowed one to understand the behaviors of other M(dmit)$_2$ salts.[157,158] They confirm the importance of tight binding methods in molecular materials. Indeed, even if ab initio calculations start to be tractable on much simple inorganic systems,[50] they are still to be improved on molecular conductors.

Finally, these compounds show that CDWs can be in competition with superconductivity in organic systems, which suggests a more conventional classical BCS mechanism of pairing.

## 5. Experimental Results: Disorder Effects

### 5.1. Introduction

Effects of impurities and defects on the physical properties of materials is an important field of investigation in condensed matter physics. In this section, we will restrict ourselves to the influence of disorder on the ground states we have described previously.

#### 5.1.1. Random Fields and Random Bounds

It is useful to start this section by introducing the random field Ising model (RFIM),[163,162] which is an intuitive model for quenched disorder. The system

of Ising variables already introduced in section 2.4 is perturbed by the presence of quenched random fields $h_i$, such that

$$\langle h_i h_j \rangle = \delta_{ij} {h_0}^2 \tag{5.1}$$

which couples linearly to the pseudospin variables in the following way:

$$H = -\frac{1}{2}\sum_{i,j} J_{ij} S_i S_j - \sum_i h_i S_i \tag{5.2}$$

The $J_{ij}$ constants can also be random: this is the random bond Ising model (RBIM). This model is used to study spin glasses.[165] In that case, the $J_{ij}$ constants are randomly positive (ferromagnetic-like) or negative (antiferromagnetic-like), which generates a *frustration*. This mean-field RBIM of Sherrington−Kirkpatrick[166] has been used to interpret experiments on disordered molecular conductors (see section 5.3).

The RFIM is well adapted to different types of materials, like disordered magnetic systems[164] or molecular conductors in the presence of quenched disorder. In the following, we will only consider cases were the $J_{ij}$ conplings are limited to first neighbors (we will note in particular $J_{ij} = \delta_{i+1,j}J$). The first characteristic of this kind of model is the competition between two energies: the exchange energy $J$, which favors long-range order, and the field energy, which favors the local ordering of the spins. Two limits have to be distinguished:

(1) The *strong* field (strong pinning) limit $h_0 \gg J$, in which each field polarized a domain around it. Long-range order is impossible, and there is no phase transition.

(2) The *weak* field (weak pinning) limit, for which the existence of a phase transition depends on the dimensionality of the space $D$. In the $d = 1$ Ising case, Imry and Ma[173] have proposed that if $D \leq 2$, the systems will break into finite size domains, with the domain wall energy being compensated by the field energy gained by placing domains strategically. If $D > 2$, the creation of such domains is not favorable and long-range order settles in. Over the years, the "domain argument" of Imry and Ma has been improved[174,175] and the result well established: for the $d = 1$ Ising model the critical dimension below which no phase transition occurs is $D_c^1 = 2$.

For a $d = 2$ order parameter, like $XY$ spins, the domain argument can be used and give a critical dimension $D_c^1 = 4$,[176−178] indicating that, in *real* systems, no LRO is expected. This case, which can also model the pinning of vortices in superconductors, corresponds to pinning of incommensurate CDWs.[179] To briefly summarize the theoretical results, let us recall that, in a $2k_F$-CDW state (the reasoning would be the same for SDWs, CDWs, or BOWs, with $2k_F$ or $4k_F$ wave vectors), the charge density reads

$$\rho(\mathbf{r}) = \rho_0 + \delta\rho \sin(2\mathbf{k}_F\cdot\mathbf{r} + \varphi(\mathbf{r})) \tag{5.3}$$

The first model of CDW pinning was proposed by Fukuyama, Lee, and Rice (FLR).[176−178] In this model, only the phase variations of the CDW are considered because, at low temperature, the amplitude excitations are too high in energy to be excited. This has been confirmed by inelastic neutrons[47] and X-ray measurements[187] on blue bronze $K_{0.3}MoO_3$. The CDW is considered as an elastic medium, characterized by two elastic constants, $C_{\|}$ and $C_{\perp}$, in the chain direction and transverse to the chains, respectively. The elastic part of the Hamiltonian reads

$$\mathscr{H}_{el} = \int d^3\mathbf{r}\, (C_{\|}/2(\partial_x\varphi)^2 + C_{\perp}/2(\partial_{\perp}\varphi)^2) \tag{5.4}$$

The Hamiltonian of interaction between the CDW and the impurities reads, in direct space and in Fourier space,

$$\mathscr{H}_{imp} = \sum_m \int d^3\mathbf{r}\, v(\mathbf{r} - \mathbf{r}_m)\, \rho(\mathbf{r}) = \sum_m \sum_{\mathbf{q}} v_{\mathbf{q}} \rho_{-\mathbf{q}} e^{i\mathbf{q}\mathbf{r}_m} \tag{5.5}$$

where $v(\mathbf{r} - \mathbf{r}_m)$ is the potential of interaction of an impurity at the site $\mathbf{r}_m$, and $v_{\mathbf{q}}$ and $\rho_{\mathbf{q}}$ are the FTs of $v(\mathbf{r})$ and $\rho(\mathbf{r})$, respectively.

For a CDW, two terms dominate this equation:[184,185,197]

(1) The *bakscattering* term at $\mathbf{q} \sim \pm 2\mathbf{k}_F$ is responsible for the pinning of the CDW phase on the impurity. In the FLR model, where the impurity potential is supposed to have the simple form $v(\mathbf{r} - \mathbf{r}_m) = U\delta(\mathbf{r} - \mathbf{r}_m)$, this term dominates eq 5.5. It has strong consequences for the structural features of molecular conductors, as we shall see in section 5.4.

(2) The *forward scattering* term at $\mathbf{q} \sim 0$ is responsible for phase *deformation* around impurities in order to screen the charge impurity, acting like low-temperature Friedel oscillations.[186] This term alters the shape of the CDW peaks, which has been observed in inorganic systems,[188] but in molecular compounds, no clear effect has been measured, so far.

As for the RFIM, there are two kinds of pinning, which depend on the relative importance of the elastic term (eq 5.4) and the interaction term (eq 5.5), which are in competition: strong pinning is expected when the interaction energy dominates; weak pinning is expected otherwise. In the strong pinning case the CDW phase $2\mathbf{k}_F\cdot\mathbf{r} + \varphi(\mathbf{r})$ is the same at all impurity sites. An experimental illustration of strong pinning will be given in section 5.4. When elastic energy dominates, the situation is more subtle. The Imry−Ma domain argument was first presented, and the CDW ground state was thought of as an assembly of domains of constant phase $\varphi(\mathbf{r})$, called Lee−Rice domains. But this description proved to be incomplete. In a 3D system, the region in which the phase changes has to be as small as possible.[189] Theoretical works then considered a structure with small and large scale variations.[189−191] Other authors[192,193] have stressed the importance of Friedel oscillations around impurities, and the importance of their *phase shift*.[197]

Finally, this problem of CDW pinning has been revisited recently, due to its similarity with vortices' pinning in superconductors.[180,181] The ground state of the weak pinning case is described by a Bragg glass,[182−185] in which vortices' positions (or the CDW phase) have a quasi-long-range order (QLRO) for

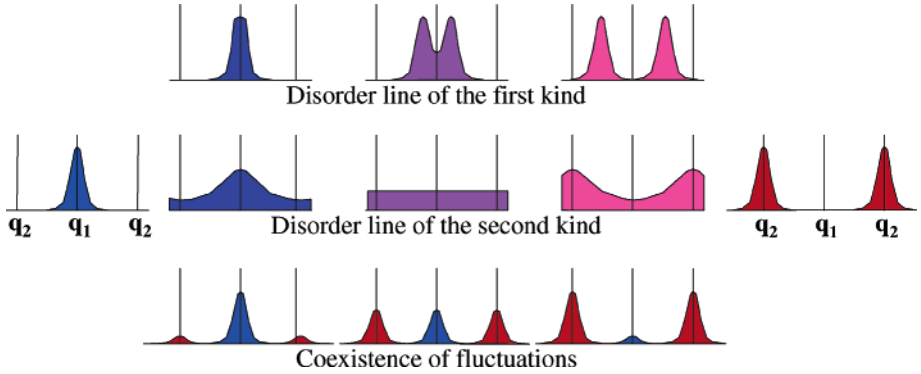


**Figure 14.** Schematic representation of the diffuse scattering, in three processes for the $\mathbf{q}_1$-SRO (blue) into $\mathbf{q}_2$-SRO (red) transformation.

distances larger than the Lee−Rice domain sizes. (In quasi-long-range order, correlation functions have power laws instead of exponential ones for SRO.) No phase defects such as CDW dislocations are expected in this phase.

The consequences of these concepts for scattering experiments are important. First of all, note that in RFIM models the order parameter correlation function is predicted to decrease exponentially, either in the strong field case[162] or in the weak field case.[195] Lorentzian squared line shapes are thus expected in three dimensions. This has been observed in high-resolution synchrotron studies performed on the AO transition of $(TMTSF)_2ClO_4$.[169] The effects of the RFIM (and RBIM) on disordered $(TM)_2X$ compounds will be discussed in section 5.3.

In the CDW cases, though Lorentzian squared line shapes are also expected in strong pinning, the situation is more complex in weak pinning. At short distance, an exponential decay is predicted,[194] leading to Lorentzian squared wings in Fourier space, while the QLRO expected should give diverging peaks, with power law exponents.[184,185,213] This latter feature has never been observed so far.

Nevertheless, it is now well-established that CDW long-range order is destroyed by impurities, as predicted by the above-mentioned theories. Indeed, diffraction experiments clearly show that introduction of disorder broadens the $2k_F$ satellite reflections, either in blue bronze,[196−198] $NbSe_3$,[199−202] or in molecular conductors, as we shall see. Moreover, squared Lorentzian line shapes are usually observed, showing that the Lee-Rice domain image is relevant. In section 5.4 we will present a situation in which the strong pinning in clearly observed.

### 5.1.2. Disorder Lines

To conclude this brief introduction to structural effects of disorder, let us discuss the issue of short-range order competition. From the Landau theory of phase transition, we know that when different long-range orders are present in a generalized phase diagram, the separating lines are first- or second-order transition lines. Is there a line separating the SROs corresponding to these phases? In other words, how do the short-range orders transform into each other? There is no clear answer to this question, but it has to do with disorder lines, a concept introduced by Stephenson from the exact solution of the Ising model.[203,204]

Let us consider two ordered phases, characterized by the reduced wave vectors $\mathbf{q}_1 = (0, 1/2)$ and $\mathbf{q}_2 = (1/2, 1/2)$. At higher temperature (say), the corresponding SRO will give rise to diffuse scattering centered at these reduced wave vectors. Phenomenologically, three transformation processeses from the $\mathbf{q}_1$-SRO to the $\mathbf{q}_2$-SRO can occur, as depicted in Figure 14. This classification is not rigorous but relies on experiments performed on molecular systems. The transformation can occur through

(1) a disorder line of the first kind. In this situation, the $\mathbf{q}_1 = (0, 1/2)$ peak first becomes squared Lorentzian (on the disorder line) and then splits into two incommensurate scatterings (on a so-called Lifschitz line[109,205]), which then shift toward the $\mathbf{q}_2$-SRO.

(2) a disorder line of the second kind, in which the systems *disorder* before changing of the SRO.

(3) a coexistence of SROs. The $\mathbf{q}_1$-peak disappears gradually, while the $\mathbf{q}_2$ one emerges. There are no disorder lines.

The physical origin of disorder lines is the existence of microscopic competing interactions in the systems. Diffuse scattering typical of disorder lines has been observed in substituted perylene salts, as discussed in the next section. Coexistence of fluctuations is more usual and has been observed in disordered $(TM)_2X$ salts.

## 5.2. Disorder Study in Substituted Perylene Salts

The polyarene has given rise to interesting families of molecular conductors.[206] The substituted perylene radical cations CPP (1,2,7,8-tetrahydrodicyclopenta-[*cd*,*lm*]perylene) and TMP (3,4,9,10-tetramethylperylene) have been synthesized, and 2:1 charge-transfer salts of general formula $(M)_2X-S$ have been obtained, with M = CPP or TMP, X = $PF_6$ or $AsF_6$, and S = $CH_2Cl_2$.[108,109] These isostructural salts (monoclinic space group $C2/m$) consist of stacks of radical cations in the **c** direction, separated by chains of alternating X and S molecules (X/S chains). These compounds are quarter-filled, as all 2:1 charge-transfer salts. At room temperature CPP salts are slightly more conducting $(50\ (\Omega\ cm)^{-1})$ than those of TMP $(5\ (\Omega\ cm)^{-1})$. CPP salts undergo a Peierls transition (at 158 and 170 K for the $PF_6$ and $AsF_6$ salts, respectively) with the stabilization of a $\mathbf{q}_P = (0, 1/2, 1/2)$ superstructure.

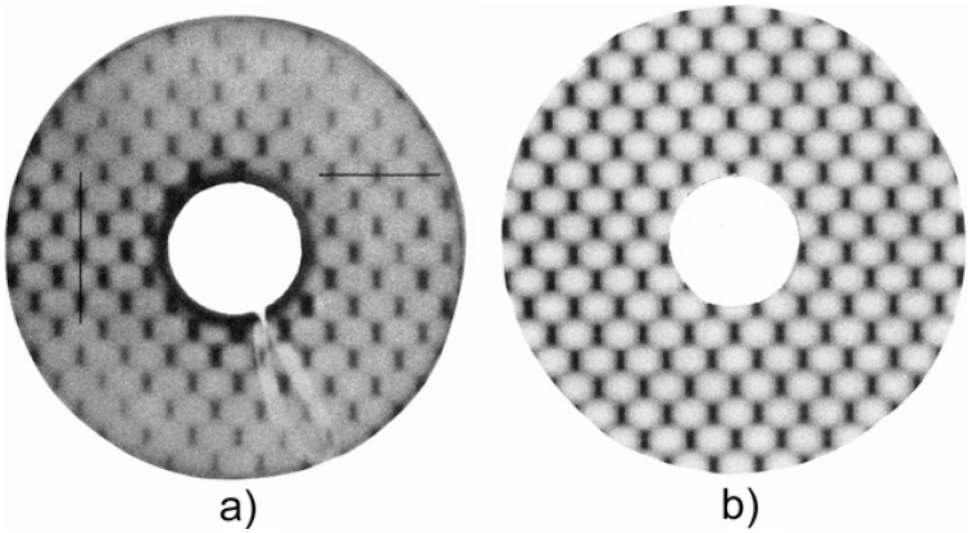


**Figure 15.** (a) Precession pattern ($\lambda_{CuK\alpha}$) of the $l = 1/2$ reciprocal plane of $(TMP)_2AsF_6CH_2Cl_2$ and (b) its best simulation.

In TMP salts, $2k_F$ diffuse lines appear below 200 K but never condense down to 20 K. Interestingly enough, $^{13}C$ NMR measurements clearly show 14 locally resolved $^{13}C$ Knight-shift sets and only 7 lines in CPP, as expected by symmetry. As we mentioned in section 4.1, this is a signature of the presence of a $4k_F$-CDW.

X/S chains were found to have two symmetrical positions in the unit cell. In the CPP salts all X/S chains were 3D ordered in their channels. However, in TMP salts a complex disorder was observed. Figure 15 represents a typical X-ray diffuse scattering pattern of $l = 1/2$ obtained in $(TMP)_2AsF_6CH_2Cl_2$. This pattern cannot be understood by classical concepts such as those described in section 2.4, because it is characteristic of a system close to a disorder line of the first kind. Indeed, the configuration of the X/S chains is due to the direct electrostatic interactions between the chains and to indirect interactions through the molecular chains in the two possible directions **a** and **b**. Such a strange X-ray pattern has been correctly simulated (Figure 15) from an Ising model with competing interactions between X/S chains.

Consequently, it has been suggested that, in the CPP salts, the absence of disorder is due to the screening of these mediated interactions by the electron gas of the CPP chains. In TMP, the $4k_F$-CDW charge localization prevents this screening and the competing interactions disorder the A/S sublattice. This example confirms that, in molecular conductors, very tiny differences in the radical cation properties (electrochemical measurements show that the intramolecular Coulomb repulsion could be estimated to be 0.65 and 0.56 eV for TMP and CPP, respectively[108]) can lead to very different ground states.

Finally, let us point out again that, in this case, the $4k_F$-CDW clearly competes with the $2k_F$-BOW, as was suggested in section 4.1.

## 5.3. Disorder Effects in $(TM)_2X$

Disorder effects in $(TM)_2X$ salts have been studied in three different compounds: the anionic solid solutions $(TM)_2X_xY_{1-x}$, the molecular solid solutions

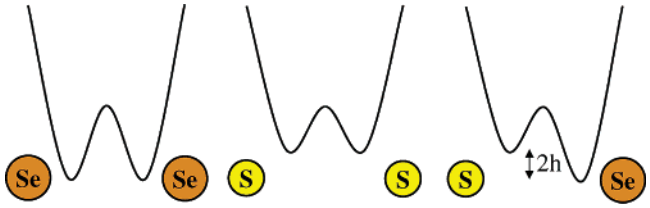


**Figure 16.** Schematic representation of the potential experienced by an anion in a Se−Se (left), S−S (center), or S−Se (right) environment (see also Figure 7).

$(TMTTF)_x(TMTSF)_{1-x}X$, and the series $(TMDTDFS)_2X$, where TMDTDSF is the hybrid S−Se molecule (see next section).

A key point to understand disorder in $(TM)_2X$ is that the electrostatic potential experienced by an anion depends on its environment, as depicted in Figure 16. As indicated in Figure 7, anions have short contacts with two neighboring molecules, related by a symmetry center. When these molecules are the same, the potential is symmetric. When the molecules are different, as in solid solutions, the potential is asymmetric and can be modeled by adding the effect of a field $h$, which is random if the disorder is random. On the other hand, when anions order with different wave vectors (see Table 2), as is the case for the same anion in different environments ($ClO_4$ in TMTTF and TMTSF salts) or for different anions in the same environment ($ClO_4$ and $ReO_4$ in TMTSF salts), the interactions between anions will be modeled by random bonds. This will be discussed in the next three sections.

### 5.3.1. Disorder Effects in TMDTDSF Salts

The molecule TMDTDSF (tetramethyldithiadiselenafulvalenium) is a hybrid between the TMTSF and TMTTF molecules[152,153] (see Figure 1). $(TMDTDSF)_2X$ salts isostructural to the Bechgaard and the Fabre salts have been synthesized with X = $PF_6$, $AsF_6$, $SbF_6$, $ReO_4$, $BF_4$, and $ClO_4$, as a link to the selenium- and sulfur-based families.

The TMDTDSF molecules are not centrosymmetric and can take two orientations on the same site. The resulting static orientational disorder has been fully

characterized[159] by the study of the X-ray diffuse scattering. Indeed, this type of orientational disorder gives rise to a Laue scattering, well described by formula 2.12. Due to the large difference of electrons between S and Se, the contrast term $\Delta F$ is very strong and gives large clouds of diffuse scattering. It has been shown that the orientation of the molecules is random, which means that no preferential orientation toward the anion was observed and that there is no correlation between orientations of neighboring molecules. However, as expected from the difference of size between S and Se, the molecules slightly move in the **a** direction in order to accommodate the difference of size of atoms in close contact. This size effect, which is due to a coupling between the orientational and the displacement disorder, gives rise to asymmetry in the diffuse scattering described by the term in eq 2.13. The displacements are estimated at about 0.10(5) and 0.03(1) Å for first- and second-neighbor molecules, respectively. The first-neighbor size effects amount to the dimerization amplitude of the organic stacks in the $(TMTTF)_2X$ family but are larger than that of the Bechgaard salts.

The results for octahedral anions have already been discussed in section 4.1. The AO characteristics of $(TMDTDSF)_2X$ are summarized in Table 2. In the case of the $ReO_4$ anion, a phase transition is observed, at a temperature which is the exact average of that of TMTTF and TMTSF salts. As the wave vectors are the same for both series, only random fields contribute to the disorder. The LRO observed in the $ReO_4$ salt suggests a weak coupling situation ($h_0 < J$). At variance, the quasi-phase transition observed in the $BF_4$ salts indicates that the random fields dominate the couplings ($h_0 > J$). Finally, for the $ClO_4$ salt only ($^1/_2$, $^1/_2$, $^1/_2$) SRO is observed. In that case, random fields and random bonds kill the anion ordering.

### 5.3.2. Solid Solutions $(TMTSF)_2(ReO_4)_{1-x}(ClO_4)_x$

These solid solutions were prepared in order to study the competition between anion orderings of different periodicities: the $\mathbf{q}_1 = (^1/_2, ^1/_2, ^1/_2)$ AO of $(TMTSF)_2ReO_4$ and the $\mathbf{q}_2 = (0, ^1/_2, 0)$ AO of $(TMTSF)_2ClO_4$. The random character of the solid solution was checked by studying the resulting Laue scattering.[161] The results are summarized in Figure 17.

True phase transitions, leading to LRO, are observed on the $ReO_4$-rich side of the phase diagram ($x < 0.5$). This is consistent with the observation of a clear energy gap in the $x = 0.35$ compound.[168] On the $ClO_4$-rich side, LRO exists for $x > 0.97$, together with superconductivity.[168] For $x < 0.97$, $\mathbf{q}_2$-SRO suppresses the superconductivity and stabilizes the $2k_F$-SDW ground state.[168] This effect is similar to the quench of the $\mathbf{q}_2$-AO in pure $(TMTSF)_2ClO_4$, where the reduction of the $\mathbf{q}_2$-ordered domains due to rapid quenching destabilizes the superconductivity, to the benefit of the $2k_F$-SDW.[169] For the intermediate concentrations $0.72 < x < 0.97$, *coexisting* SROs are clearly observed, in a way corresponding to the third process defined in section 5.1.2. The absence of disorder lines has been ascribed to the different mechanisms involved in the AO, driven by the electron gas in the $ReO_4$ salt and by direct electrostatic interactions in the $ClO_4$ one.

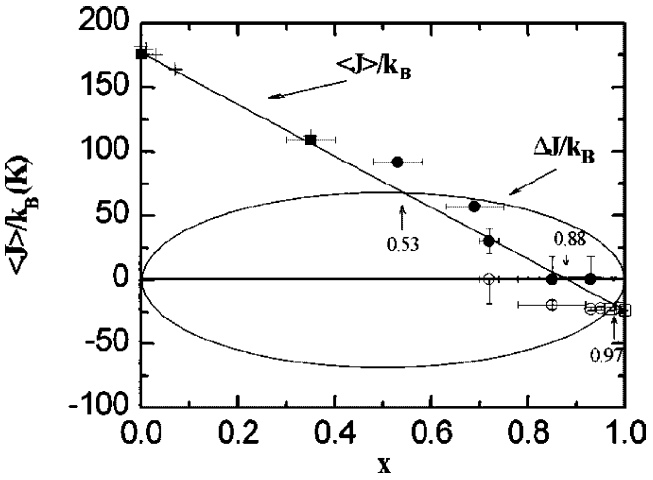


**Figure 17.** Phase diagram ($T$, $x$) of the solid solutions $(TMTSF)_2(ReO_4)_{1-x}(ClO_4)_x$. For the reasons explained in the text, the transition temperatures have been chosen negative on the $ClO_4$-rich side and positive on the $ReO_4$-rich side. Squares correspond to LRO phase transitions, while circles indicate the occurrence of SRO.

Surprisingly, this phase diagram is well accounted for by the RBIM mean-field model of Sherrington and Kirkpatrick.[166] In this model, the coupling constants are taken to be equal to the transition temperatures, considering positive constants if the coupling is antiferro-like (in all the directions of $ReO_4$) and negative ones if the order is ferro-like (in the **a** and **c** directions of $ClO_4$). (Note that, for the sake of presentation, the sign conventions of the coupling constants have been changed here.) Here $J_1 = 176$ K and $J_2 = -24$ K. The mean interaction for a concentration $x$ is

$$\langle J\rangle/k_B \equiv (1-x)J_1 + xJ_2 = 176 - 200x \quad (5.6)$$

and its root-mean-square $\Delta J$ is

$$\Delta J/k_B \equiv \sqrt{\frac{x(1-x)}{2}}|J_2 - J_1| = 200\sqrt{\frac{x(1-x)}{2}} \quad (5.7)$$

The model predicts[167] a phase transition if $|\langle J\rangle| > \Delta J$ and a vitreous phase in the case of $|\langle J\rangle| < \Delta J$.

The curves $\langle J\rangle/k_B(x)$ and $\Delta J/k_B(x)$ are represented in Figure 17. Their intersection points $x_1 = 0.53$ and $x_2 = 0.97$, between which SRO is predicted, are close to the experimental values.

### 5.3.3. Solid Solutions $(TMTSF)_{1-x}(TMTTF)_xReO_4$

The last type of disorder studied in $(TM)_2X$ salts concerns the solid solutions TMTTF/TMTSF. Earlier studies had mostly focused on the low-$x$ concentration limit of the $PF_6$[207] and $ClO_4$ salts.[208] A general study of the solid solution $(TMTSF)_{1-x}(TMTTF)_xReO_4$ has been performed on the whole $x$ range,[116] showing that the electronic and structural properties do not behave monotonically with $x$.

The main observation is that the molecules are not randomly distributed but tend to alternate and to form a well-defined structure, characterized by the

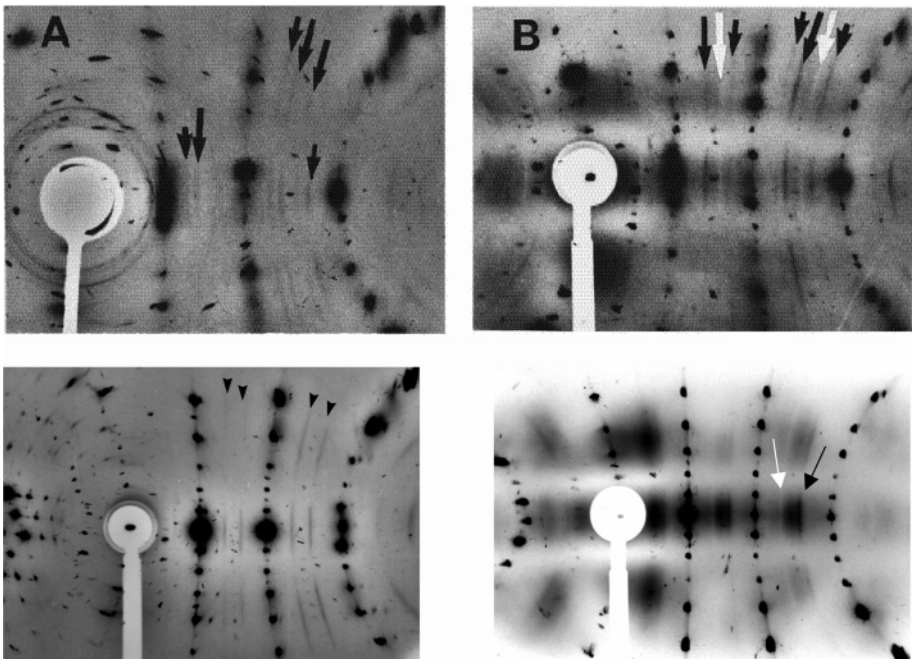


**Figure 18.** Diffraction patterns ($\lambda_{CuK\alpha}$) from (top) TTF-TCNQ at 60 K (A) and $TTF_{0.97}TSF_{0.03}$-TCNQ at 40 K (B) [Small and large black arrows point toward $2k_F$ and $4k_F$ lines.] and (bottom) HMTSF-TCNQ at 25 K (left) and $HMTTF_{0.05}HMTSF_{0.95}$-TCNQ at 20 K (right) [Black arrows point toward $2k_F$ lines. White arrows point toward $4k_F$ lines.].

(0, $^1/_2$, $^1/_2$) wave vector. In the $x \sim 0.55$ compound, which is closer to the perfect $^1/_2$ composition, the alternate order extends to ~300 Å in the chain direction, while $x \sim 0.2$ and ~0.8 solid solutions only exhibit local order. The alternation of the molecules induces a strong (~0.2 eV) $4k_F$ potential along the chain, very similar to a $4k_F$-CDW.

At variance with the $(TMDTDSF)_2ReO_4$ salt, for which the anion ordering transition is intermediate between that of $(TMTSF)_2ReO_4$ and $(TMTTF)_2ReO_4$, the $x = 0.55$ compound undergoes the AO transition at 75 K. The interpretation of this strong decrease of the transition temperature is that the $2k_F$-BOW response function driving the ($^1/_2$, $^1/_2$, $^1/_2$) anion ordering is decreased by the occurrence of the $4k_F$-CDW due to the molecule ordering. Qualitatively, the "heteropolar" distribution of charge diminishes the resonating character of the $2k_F$-BOW response function.[72,73,90] This is consistent with many features observed in charge ordered compounds (see section 4.1.4).

## 5.4. Pinning of Charge-Density Waves

The properties of 1D solids change drastically when disorder is introduced. In incommensurate $2k_F$-BOW states, for example, a non-ohmic extracurrent is measured when the electric fields are larger than a threshold value.[41] This nonlinear conductivity, discovered in $NbSe_3$,[170] has also been observed in the blue bronze $K_{0.3}MoO_3$[171] and even in the $2k_F$-SDW of $(TMTSF)_2NO_3$.[172] The physical origin of this extracurrent is the sliding of the density wave: it is a collective effect. The threshold field is due to the pinning of the CDW on defects or impurities always present in real materials. Though the loss of LRO is clearly established experimentally, microscopic information on the pinning mechanism in the vicinity of the impurity is difficult to obtain. However, in solid solutions such as $(TTF)_x(TSeF)_{1-x}$-TCNQ, the observation of the intensity asymmetry effect described in section 2.3 demonstrates the existence of strong pinning around the substituent molecules.

The $(TTF)_x(TSF)_{1-x}$-TCNQ and $(HMTTF)_x(HMTSF)_{1-x}$-TCNQ solid solutions were studied by the so-called *Laue monochromatic* or fixed-film fixed-crystal method.[12,210,211] (In the following these chemical formulas will be noted $(TF)_x$ and $(HF)_x$.) Figure 18 displays a set of X-ray photographs of a pure compound in its 1D fluctuating regime and of the same compound substituted. In TTF-TCNQ, diffuse lines are clearly seen at $2k_F = 0.295b^*$ and $4k_F = 0.59b^*$. These $2k_F$ and $4k_F$ lines are visible between 52 and 150 K and between 45 and 300 K, respectively.[7] In the solid solution $(TF)_{x=0.97}$, these lines are also observed. But contrary to the case of the pure compound, the diffuse line at $+4k_F$ appears in white in the photograph. (Although it is more convenient to use the $\pm 4k_F$ notation to describe the photographs of Figure 18, the best way to define the position of a line is by its angular position with respect to the closer Bragg reflection. Indeed, because of the Friedel law, a line located at small angles with respect to the Bragg layer is at $+4k_F$ on the left side of the photograph but at $-4k_F$ on the right side.) The $2k_F$ diffuse lines do not show this effect. In $(HM)_{x=0.05}$, the white lines are visible at $+2k_F$. Note that this effect has been observed on the $2k_F$ *and* $4k_F$ diffuse lines in a solid solution enriched in HMTTF, $(HM)_{0.87}$.[211] The photographs also exhibit a diffuse background consisting of three broad horizontal stripes. This diffuse scattering is the Laue scattering $I_{sub}$ (eq 2.11) due to the substitutional disorder between S- and Se-based molecules. As the molecules contain four chalcogen atoms, the contrast term $\Delta F$ of eq 2.11 is very strong, which explains the high intensity of the Laue

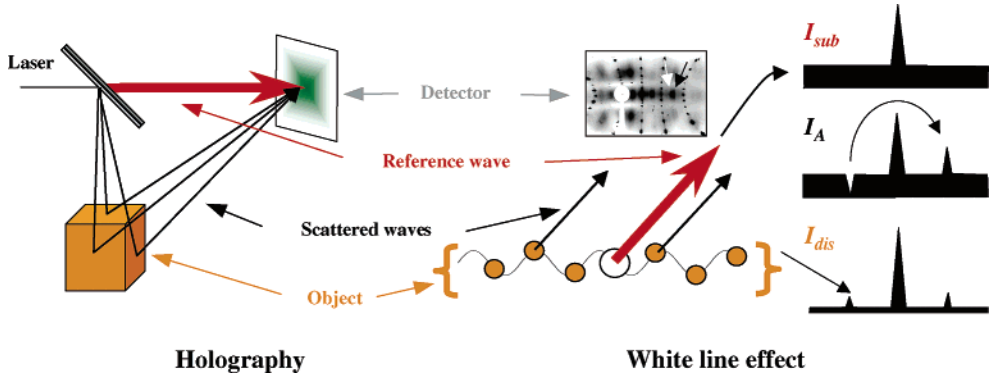


**Figure 19.** Schematic representation of the white line effect and its analogy with holography.

scattering. At last, let us note that all the white lines are observed on the large angles side.

As we shall see, this is due to a coupling between the CDW periodic distortion and the substitutional disorder, that is, to the pinning of the CDW. It is a direct consequence of the asymmetric (or holographic) term given by eq 2.13.

First of all, let us remark that the effect allows one to identify the type of chain (donor or acceptor) originating the CDW. The observation of white lines demonstrates that (1) the HTTSF chain undergoes the $2k_F$ instability, (2) the HMTTF chain undergoes both the $2k_F$ and $4k_F$ instabilities, and (3) the TTF chain undergoes the $4k_F$ instability. Such an evolution confirms that Coulomb repulsions are larger in S-based molecules because these molecules are less polarizable according to the HMTSF−HMTTF−TTF sequence.[7] In the case of $(TF)_x$ solid solution, the absence of $2k_F$ white lines confirms that this instability develops on the TCNQ chains.

Whites lines are observed in the whole temperature range (300−25 K), which means that the 3D order is not stabilized. This is consistent with the loss of long-range order observed in all CDW systems. The width of the lines is larger than the experimental resolution, which indicates a short-range order in the chain direction. From this width, one finds a correlation length $\xi \sim 40 \pm 7$ Å in the $(TF)_{x=0.97}$ case above 50 K. In $(HF)_{x=0.05}$, this correlation length is $\xi \sim 60$ Å. The CDW is thus coherent in a region comparable to the average distance between impurities, which is ~78 and 125 Å in $(HF)_{x=0.05}$ and $(TF)_{x=0.97}$, respectively. This result, together with the observation of white lines, demonstrates unambiguously the presence of strong pinning in these solid solutions. It is one of the strongest pieces of evidence of this phenomenon in CDW systems. Let us now come back to the interpretation of the asymmetry effect.

Although more complicated models can be invoked,[210] the white line effect can be explained in a simple way. Note that this interpretation was confirmed by numerical[212] and analytical calculation.[213] Let us consider a solid solution of molecules in which each impurity at position $\mathbf{r}_i$ pins a lattice distortion given by

$$\mathbf{u}(\mathbf{r}) = \mathbf{u}_0 \sin(2\mathbf{k}_F\cdot(\mathbf{r} - \mathbf{r}_i) + \varphi_0) \qquad (5.8)$$

In this expression $\varphi_0$ is the phase of the distortion *at the* impurity site. By using the formalism of section 2.3, one finds that the diffuse scattering intensity is the sum of three terms: (1) the Laue scattering (eq 2.11), proportional to the contrast term squared $\Delta F^2$ and the impurity concentration (This term gives the diffuse background.), (2) the $2k_F$ scattering (eq 2.12), proportional to the average structure factor squared $\bar{F}^2$ and to the amplitude of the distortion squared $u_0^2$ (This term is negligible here.), and (3) the asymmetric scattering term $I_A$ (eq 2.13), which in this case reads

$$I_A(\mathbf{Q} = \mathbf{Q}_{hkl} \pm 2\mathbf{k}_F) \sim \mp\bar{F}\Delta F(\mathbf{Q}\cdot\mathbf{u}_0)\cos\varphi_0 \qquad (5.9)$$

The latter term transfers intensity from one side of the Bragg spots to the other, as indicated in Figure 19. Moreover, $I_A$ is proportional to the cosine of the pinning phase $\varphi_0$. The sign of this variable can thus be determined by the white line effect. The results are indicated in Figure 20. For host materials rich in S-based (Se-based) molecules, $\varphi_0 = 0$ ($\varphi_0 = \pi$). As the electron density $\rho(x)$ is in quadrature with the displacive modulation $u(x)$ [Because the electron density increases when two molecules come closer, one has $\rho \sim -(du/dx)$.], the phase of $\rho(x)$ on the impurity site can be deduced. $\rho(x)$ and $u(x)$ are indicated in Figure 20.

As we mentioned in section 2.3, there is an elegant way to understand the white line effect based on holography and pictured in Figure 19. The principle of holography is to register the interference between a reference wave of amplitude $A_{ref}$ and a wave scattered by an object of amplitude $A_{object}e^{i\Phi}$. The total intensity is given by

$$I_{Holo} = A_{ref}^2 \qquad (5.10)$$

$$+ A_{ref}A_{object}e^{-i\Phi} + CC \qquad (5.11)$$

$$+ A_{object}^2 \qquad (5.12)$$

If the reference wave is more intense than the diffracted one ($A_{ref}^2 \gg A_{object}^2$), which is the necessary condition for holography to work, the information on the phase $\Phi$ will not be lost, because $A_{ref}^2$ is well-known. It is easy to see that the three terms of eq 5.12 represent the substitutional, the asymmetric, and the displacive terms for the pinned CDW problem. The reference wave is the X-ray scattered by the impurity, and the object is the CDW itself. As the intensity scattered by the CDW is negligible, the

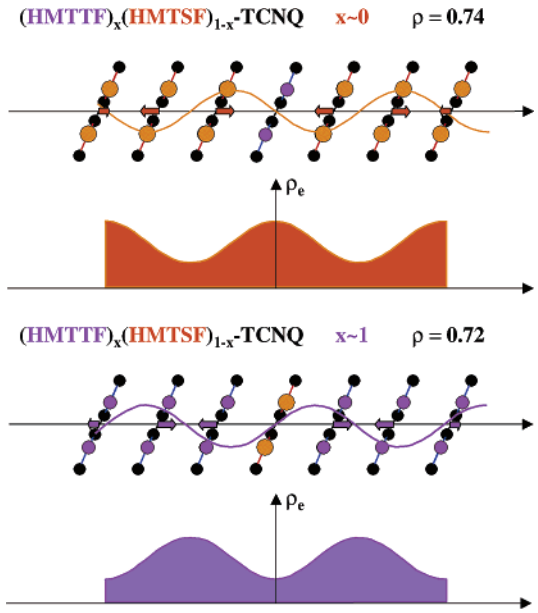


**Figure 20.** Schematic representation of the molecular displacements in the vicinity of an impurity molecule. The colored curves are the corresponding variations of the charge densities.

holographic term dominates the diffraction and the phase is retrieved.

The previous results give the following conclusions:

(1) In the vicinity of the impurities, the phase of the lattice distortion satisfies the size effects. If the impurity is smaller (larger) than the host molecules, they get closer (push away) from the impurities. This allows the constraints on the material to relax. This gain of elastic energy can be considered as a pinning mechanism of CDWs.[12]

(2) The CDW pins such that the electronic density decreases on the less electronegative molecule. As indicated by the charge-transfer values of pure HMTSF-TCNQ and HMTTF-TCNQ, 0.74 and 0.72, respectively, Se-based molecules are better donors than S-based ones. This is consistent with the fact that the electron density is minimum on the HMTSF impurity. This is a mechanism similar to the screening by Friedel oscillations. In conclusion, the white line effect is an unique effect which (i) gives unambiguous evidence of strong pinning in TTF alloys and (ii) allows one to determine the phase of the CDWs on the impurity sites. The value of this phase is consistent with elastic and electronic mechanisms of pinning.

## 6. Concluding Remarks

It is surprising that, after 30 years of study of molecular conductors, new phenomena are still being discovered and some of the most fascinating properties of these system still remain unexplained. As far as the structural properties are concerned, the complexity of the new states observed (CO, mixed states) clearly asks for a more synthetic theory of the ground states. In this respect, the interplay between structural (inter- and intramolecular modes, anion displacements, and/or orientations) and electronic (1D instabilities, electron correlations) degrees of freedom makes this task especially difficult. Although theories are mature enough to formally explore complex phase diagrams, the relevant parameters at the origin of the experimental ones are still missing.

In this review, we have shown that X-ray scattering is an indispensable method to unveil novel properties. In $(TM)_2X$, subtle states mixing spin- and charge-density waves have been discovered by X-ray diffraction. The observation of weak diffuse lines in numerous systems, including metallic or more localized ones, clearly indicates the importance and the continuity of the $2k_F$ instabilities of the 1D electron gas throughout the different families of molecular conductors. The recent discovery of charge ordering on the left side of the $(TM)_2X$ phase diagram allows one to expect a unified view of the different families of molecular conductors. Again, relevant parameters are missing to achieve such a goal. The synthesis of materials with similar structures, including solid solutions, has clearly brought valuable information on such parameters and reinforced the close collaboration with chemists and physicists in the field.

Among the little explored paths to progress in this direction, high-resolution X-ray diffraction could provide valuable information on charge-density, through precise structure determination. Such techniques should be more accessible with the development of third generation synchrotron sources. Other essential techniques, like inelastic and magnetic neutron scattering, have not been carried out yet due to the small size of the crystals. The study of structural transition dynamics and magnetic structures of molecular conductors could be as surprising as previous studies.

Finally, molecular conductors can be considered as model systems and, despite the difficulties, we can expect from their study a deeper understanding of low-dimensional and strongly correlated systems.

## 7. Acknowledgments

This review could not have been written without the close collaboration with J.-P. Pouget, R. Moret, P. Foury-Leylekian, V. Ilakovac, Q. Liu, and S. Rouzière. Fruitful collaborations with P. Auban-Senzier, P. Batail, C. Bourbonnais, K. Boubekeur, S. Brazovskii, L. Brossard, E. Canadell, C. Coulon, J.-M. Fabre, T. Garel, D. Jérome, I. Johannsen, A. Moradpour, P. Monceau, C. Pasquier, S. Tomić, and L. Valade are greatly acknowledged.

## 8. Note Added after ASAP Posting

This paper was posted ASAP on 10/27/04. The Debye−Waller factor in the paragraph under eq 2.6 was corrected. A change was made to the compound notation in the last full paragraph on the fifth page, in the heading for section 4.3, in section 5.3.1, and in the first paragraph of section 5.4. Changes were made in eqs 3.3 and 3.12 and in the text under eq 3.3. A wording change was made in the last paragraph of section 4.2 and the first paragraph of section 5.4. Reference 99 was updated. The paper was reposted on 10/28/04.

## 9. References


(1) James, R. W. *The optical principle of X-ray diffraction*; Ox-Bow Press: Woodbridge, CT, 1984.
(2) Warren, B. E. *X-ray Diffraction*; Addison-Wesley Publishing Company: Reading, MA, 1969.
(3) Guinier, A. *Théorie et Technique de la Radiocristallographie*; Dunod: Paris, 1956.
(4) Krivoglaz, M. A. *Theory of X-ray and Thermal Neutron Scattering by Real Crystals*; Plenum: New York, 1969.
(5) Dénoyer, F.; Comès, R.; Garito, A. F.; Heeger, A. *Phys. Rev. Lett.* **1975**, *35*, 445.
(6) Kagoshima, S.; Anzai, H.; Kajimura, K.; Ishiguro, T. *J. Phys. Soc. Jpn.* **1975**, *39*, 1143.
(7) For an exhautive review on the structural transitions in TTF-TCNQ and related compounds, see: Pouget, J.-P. In *Semiconductors and semimetals*; Conwell, E. M., Ed.; Academic Press: New York, 1988; Vol. 27, pp 87−214.
(8) Pouget, J.-P.; Ravy, S. *J. Phys. I* **1996**, *6*, 1501.
(9) Coppens, P. *X-ray charge density and chemical bonding*; Oxford University Press: Oxford, U.K., 1987.
(10) Sutton, M.; Nagler, S. E.; Mochrie, S. G. J.; Greytak, T.; Bermann, L. E.; Held, G.; Stephenson, G. B. *Nature* **1991**, *352*, 608.
(11) Ravy, S. *J. Phys. IV* **2002**, *12*, Pr6−7.
(12) Brazovskii, S.; Pouget, J.-P.; Ravy, S.; Rouzière, S. *Phys. Rev. B* **1997**, *55*, 3426.
(13) Guinier, A. *C. R. Acad. Sci. Paris* **1938**, *208*, 1972. Preston, G. D. *Philos. Mag.* **1938**, *26*, 855.
(14) Cowley, J. M. *Surf. Sci* **1993**, *298*, 336.
(15) Saldin, D. K.; Andres, P. L. *Phys. Rev. Lett.* **1990**, *64*, 1270.
(16) Cowley, R. A. *Adv. Phys.* **1980**, *29*, 1. Bruce, A. D. *Adv. Phys.* **1980**, *29*, 111. Cowley, R. A.; Bruce, A. D. *Adv. Phys.* **1980**, *29*, 219.
(17) Launois, P.; Ravy, S.; Moret, R. *Phys. Rev. B* **1995**, *52*, 5414. Ravy, S.; Launois, P.; Moret, R. *Phys. Rev. B* **1996**, *53*, R10532. Launois, P.; Ravy, S.; Moret, R. *Phys. Rev. B* **1997**, *55*, 2651. Launois, P.; Ravy, S.; Moret, R. *Int. J. Mod. Phys. B* **1999**, *13*, 253.
(18) Akamatsu, H.; Inokuchi, H.; Matsunaga, Y. *Nature* **1954**, *173*, 168.
(19) Kepler, R. G.; Bierstedt, P. E.; Merrifield, R. E. *Phys. Rev. Lett.* **1960**, *11*, 503.
(20) Wudl, F.; Wobschall, D.; Hufnagel, E. J. *J. Am. Chem. Soc.* **1972**, *94*, 671.
(21) Coleman, L. B.; Cohen, M. H.; Sandman, D. J.; Yamagishi, F. G.; Garito, A. F.; Heeger, A. J. *Solid State Commun.* **1973**, *12*, 1125.
(22) Ferraris, J.; Cowan, D. O.; Walatka, V.; Perlstein, J. H. *J. Am. Chem. Soc.* **1973**, *95*, 948.
(23) Peierls, R. *Quantum Theory of Solids*; Oxford University Press: London, 1955; p 108.
(24) Jérome, D.; Schulz, H. J. *Adv. Phys.* **1982**, *31*, 299.
(25) Comès, R.; Lambert, M.; Launois, H.; Zeller, H. R. *Phys. Rev. B* **1973**, *8*, 751.
(26) Wilson, J. A.; DiSalvo, F. J.; Mahajan, S. *Adv. Phys.* **1975**, *24*, 117.
(27) Pouget, J.-P. In *Low-dimensional Electronic Properties of Molybdenum Bronzes and Oxides*; Schlenker, C., Ed.; Kluwer Academic Publishers: New York, 1989.
(28) Pouget, J.-P.; Kagoshima, S.; Schlenker, C.; Marcus, J. J. *Phys. Lett.* **1983**, *44*, L113.
(29) Rouxel, J.; Schlenker, C. In *Charge Density Waves in Solids*; Gor'kov, L. P., Grüner, G., Eds.; Modern Problems in Condensed Matter Sciences; North-Holland: Amsterdam, Oxford, New York, Tokyo, 1989.
(30) Jérome, D. Organic Superconductivity 20th Anniversary. *J. Phys. IV* **2000**, *10*, Pr3−69.
(31) Jérome, D.; Mazaud, A.; Ribault, M.; Bechgaard, K. *J. Phys., Lett.* **1980**, *41*, L-95.
(32) Adachi, T.; Ojima, E.; Kato, K.; Kobayashi, H.; Miyazaki, T.; Tokumoto, M.; Kobauashi, A. *J. Am. Chem. Soc.* **2000**, *122*, 3238.
(33) Jaccard, D.; Wilhelm, H.; Jérome, D.; Moser, J.; Carcel, C.; Fabre, J.-M. *J. Phys.: Condens. Matter* **2001**, *13*, L89. Wilhelm, H.; Jaccard, D.; Duprat, R.; Bourbonnais, C.; Jérome, D.; Moser, J.; Carcel, C.; Fabre, J.-M. *Eur. Phys. J. B* **2001**, *21*, 175.
(34) Reviews on organic superconductivity can be found in: Williams, J. M.; Ferraro, J. R.; Thom, R. J.; Carlson, K. D.; Geiser, U.; Wang, H. H.; Kini, A. M.; Whangbo, M.-H. Organic Superconductors (Including Fullerenes) Synthesis, Structure, Properties, and Theory; Prentice Hall: Englewood Cliffs, NJ, 1992. Ishiguro, T.; Yamaji, K. *Organic Superconductors*; Springer Series in Solid-State Sciences 88; Springer: New York, 1990.
(35) Brossard, L.; Ribault, M.; Bousseau, M.; Valade, L.; Cassoux, P. *C. R. Acad. Sci. Paris* **1986**, *302*, 205.
(36) A review on the method and conditions required to synthesize "good" molecules can be found in: Metzger, R. M. In *Advances in Synthetic Metals, Twenty Years of Progress in Science and Technology*; Bernier, P., Lefrant, S., Bidan, G., Eds.; Elsevier: New York, 1999; p 317.
(37) The BEDT-TTF molecule was first synthesized by: Schumaker, R.; Engler, E. M. *J. Am. Chem. Soc.* **1977**, *99*, 5521. Superconductivity ($T_c = 1.5$ K, $P = 6$ kbar) was discovered in $(BEDTTTF)_2ReO_4$ by: Parkin, S. S. P.; Engler, E. M.; Schumaker, R. R.; Lagier, R.; Lee, V. Y.; Voiron, J.; Carneiro, K.; Scott, J. C.; Greene, R. L. *J. Phys.* **1983**, *44*, 791.
(38) Ravy, S.; Moret, R.; Pouget, J.-P.; Comès, R.; Parkin, S. S. P. *Phys. Rev. B* **1986**, *33*, 2049.
(39) Sólyom, J. *Adv. Phys.* **1979**, *28*, 209.
(40) Emery, V. J. In *Highly Conducting One-Dimensional Solids*; Devreese, J. T., et al., Eds.; Plenum: New York, 1979.
(41) Reviews on the Peierls transition are: (a) Grüner, G. *Density waves in Solids*; Frontier of Physics 89; Addison-Wesley: Reading, MA, 1994. (b) Pouget, J.-P. In *Physics and Chemistry of Low-Dimensional Inorganic Conductors*; Schlenker, C., Ed.; Plenum Press: New YorPhysics and Chemistry of Low-Dimensional Inorganic Conductorsk, 1996.
(42) Whangbo, M.-H.; Ren, J.; Liang, W.; Canadell, E.; Pouget, J.-P.; Ravy, S.; Williams, J. M.; Beno, M. A. *Inorg. Chem.* **1992**, *31*, 4169.
(43) Whangbo, M.-H.; Canadell, E.; Foury, P.; Pouget, J.-P. *Science* **1991**, *252*, 96.
(44) Holstein T. *Ann. Phys. (N. Y.)* **1959**, *8*, 325; **1959**, *8*, 343.
(45) Su, W. P.; Schrieffer, J. R.; Heeger, A. J. **1979**, *42*, 1648. Heeger, A. J.; Kivelson, S.; Schrieffer, J. R.; Su, W. P. *Rev. Mod. Phys.* **1988**, *60*, 781.
(46) Comès, R.; Shirane, G. In *Higly Conducting One Dimensional Solids*; Devreese, J. T., Evrard, R. P., Van Doren, V. E., Eds.; Plenum: New York, 1979; p 17.
(47) Hennion, B.; Pouget, J.-P.; Sato, M. *Phys. Rev. Lett.* **1992**, *68*, 2374. Pouget, J.-P.; Hennion, B.; Sato, M. *J. Phys. IV* **1993**, *3*, 215.
(48) Bouveret, Y.; Megtert, S. *J. Phys. (Paris)* **1989**, *50*, 1649.
(49) Lee, P. A.; Rice, M.; Anderson, P. W. *Phys. Rev. Lett* **1973**, *31*, 462.
(50) Sandré, E.; Foury-Leylekian, P.; Ravy, S.; Pouget, J.-P. *Phys. Rev. Lett.* **2001**, *86*, 5100.
(51) Voit, J. *Rep. Prog. Phys.* **1995**, *58*, 977.
(52) Voit, J. *Eur. Phys. J. B* **1998**, *8*, 505.
(53) Schulz, H. J. *Int. Mod. Phys. B* **1991**, *5*, 57.
(54) Schulz, H. J. In *Strongly Correlated Electronic Materials: The Los Alamos Symposium 1993*; Bedell, K. S., Wang, Z., Meltzer, D., Balatsky, A., Abrahams, E., Eds.; Addison-Wesley: Reading, MA, 1994.
(55) Giamarchi, T. *Physica B* **1997**, *230*, 975.
(56) Bourbonnais, C.; Jérome, D. In *Advances in Synthetic Metals, Twenty Years of Progress in Science and Technology*; Bernier, P., Lefrant, S., Bidan, G., Eds.; Elsevier: New York, 1999; p 206.
(57) Hirsch, J. E.; Scalapino, D. J. *Phys. Rev. B* **1984**, *29*, 5554.
(58) Pouget, J.-P.; Khanna, S. K.; Dénoyer, F.; Comès, R.; Garito, A. F.; Heeger, A. J. *Phys. Rev. Lett.* **1976**, *37*, 437. Kagoshima, S.; Ishiguro, T.; Anzai, H. *J. Phys. Soc. Jpn.* **1976**, *41*, 2061.
(59) Emery, V. J. *Phys. Rev. Lett.* **1976**, *37*, 107.
(60) Mazumdar, S.; Ramasesha, S.; Clay, R. T.; Campbell, D. K. *Phys. Rev. Lett.* **1999**, *82*, 1522.
(61) Hubbard, J. *Phys. Rev. B* **1978**, *17*, 494.
(62) Lieb, L. H.; Lu, F. Y. *Phys. Rev. Lett.* **1968**, *20*, 1445.
(63) Klein, D. J.; Seitz, W. A. *Phys. Rev. B* **1974**, *10*, 3217.
(64) Hirsch, J. E.; Scalapino, D. J. *Phys. Rev. B* **1983**, *27*, 7169. Hirsch, J. E.; Scalapino, D. J. *Phys. Rev. Lett.* **1983**, *50*, 1168.
(65) Hirsch, J. E. *Phys. Rev. Lett.* **1984**, *53*, 2327.
(66) Mila, F.; Zotos, X. *Europhys. Lett.* **1993**, *24*, 133.
(67) Mazumdar, S.; Campbell, D. K. *Phys. Rev. Lett.* **1985**, *55*, 2067.
(68) Ung, K. C.; Mazumdar, S.; Toussaint, D. *Phys. Rev. Lett.* **1994**, *73*, 2603.
(69) Mazumdar, S.; Clay, R. T.; Campbell, D. K. *Phys. Rev. B* **2000**, *62*, 13400.
(70) Bâldea, I.; Köppel, H.; Cederbaum, L. S. *Phys. Rev. B* **2004**, *69*, 75307.
(71) Riera, J.; Poilblanc, D. *Phys. Rev. B* **2000**, *59*, 2667.
(72) Riera, J.; Poilblanc, D. *Phys. Rev. B* **2000**, *62*, R16243.
(73) Riera, J.; Poilblanc, D. *Phys. Rev. B* **2001**, *63*, R241102.
(74) Bray, J. W.; Interrante, L. V.; Jacobs, I. S.; Bonner, J. C. In *Extended Linear Chain Compounds*; Miller, J. S., Ed.; Plenum: New York, 1983; Vol. 3.
(75) Bonner, J. C.; Fisher, M. E. *Phys. Rev.* **1964**, *135*, A640.
(76) Eggert, S.; Affleck, B.; Takahashi, M. *Phys. Rev. Lett.* **1994**, *73*, 332.
(77) Hase, M.; Terasaki, I.; Uchinokura, K. *Phys. Rev. Lett.* **1993**, *70*, 3651.
(78) Pouget, J. P.; Regnault, L. P.; Aïn, M.; Hennion, B.; Renard, J. P.; Veillet, P.; Dhalenne, G.; Revcolevschi, A. *Phys. Rev. Lett.* **1994**, *72*, 4037.
(79) For a review on $CuGeO_3$, see: Boucher, J. P.; Regnault, L. P. *J. Phys. I* **1996**, *6*, 1939.
(80) Mila, F. *Phys. Rev. B* **1995**, *52*, 4788.
(81) Jacobsen, C. S. *J. Phys. C* **1986**, *19*, 3805.

(82) Barišić, S.; Brazovskii, S. In *Recent Developments in Condensed Matter Physics*; Devreese, J. T., Ed.; Plenum Press: New York, 1981; Vol. 1, p 327. Emery, V. J.; Bruinsma, R.; Barišić, S. *Phys. Rev. Lett.* **1982**, *48*, 1039.
(83) Bray, J. W.; Hart, H. R.; Interrante, L. V.; Jacobs, I. S.; Kasper, J. S.; Watkins, G. D.; Wee, S. H.; Bonner, J. C. *Phys. Rev. Lett.* **1975**, *35*, 744.
(84) (a) Bosch, A.; Van Bodegom, B. *Acta Crystallogr.* **1977**, *33*, 3013. (b) Van Bodegom, B.; Larson, B. C.; Hook, H. A. *Phys. Rev. B* **1981**, *24*, 1520. (c) Visser, R. J. J.; Oostra, S.; Vettier, C.; Voiron, J. *Phys. Rev. B* **1983**, *28*, 2074.
(85) Huizinga, S.; Kommadeur, K.; Sawatzky, G. A.; Thole, B. T.; Kopinga, K.; de Jonge, W. J.; Roos, J. *Phys. Rev. B* **1979**, *19*, 4723.
(86) Pouget, J.-P.; Moret, R.; Comès, R.; Bechgaard, K. *J. Phys., Lett.* **1981**, *42*, L543.
(87) Pouget, J.-P.; Moret, R.; Comès, R.; Bechgaard, K.; Fabre, J.-M.; Giral, L. *Mol. Cryst. Liq. Cryst.* **1982**, *79*, 129.
(88) Coulon, C.; Delhaes, P.; Flandrois, S.; Lagnier, R.; Bonjour, E.; Fabre, J.-M. *J. Phys., Lett.* **1982**, *43*, 1059.
(89) Maaroufi, A.; Flandrois, S.; Coulon, C.; Delhaes, P.; Morand, J. P.; Filhol, A. *J. Phys., Colloq.* **1982**, *44*, C3, 37.
(90) Emery, V. J. *J. Phys., Colloq.* **1983**, *44*, C3, 977.
(91) Brazovskii, S.; Yakovenko, V. *J. Phys., Lett.* **1985**, *46*, L111.
(92) Thorup, N.; Rindof, G.; Soling, H.; Bechgaard, K. *Acta Crystallogr., B* **1981**, *37*, 1236.
(93) Ducasse, L.; Abderrabba, M.; Hoarau, J.; Pesquer, M.; Gallois, B.; Gautier, J. *J. Phys.* **1986**, *C19*, 3805. Ducasse, L.; Abderrabba, M.; Gallois, B.; Chasseau, D. *Synth. Met.* **1987**, *19*, 327.
(94) Ducasse, L.; Coulon, C.; Chasseau, D.; Yagbasan, R.; Fabre, J. M.; Gouasmia, A. K. *Synth. Met.* **1988**, *27B*, 543.
(95) Zamborsky, F.; Yu, W.; Raas, W.; Brown, S. E.; Alavi, B.; Merlic, C. A.; Baur, A.; Lefebvre, S.; Wzietek, P. *J. Phys. IV* **2002**, *12*, Pr9−139.
(96) Ribault, M.; Pouget, J.-P.; Jerome, D.; Bechgaard, K. *J. Phys., Lett.* **1980**, *41*, L607. Pouget, J.-P.; Moret, R.; Comès, R.; Bechgaard, K.; Fabre, J.-M.; Giral, L. *Mol. Cryst. Liq. Cryst.* **1982**, *79*, 129.
(97) Pouget, J. P. *Chem. Scr.* **1981**, *17*, 85.
(98) Wzietek, P.; Creuzet, F.; Bourbonnais, C.; Jerome, D.; Bechgaard, K.; Batail, P. *J. Phys. I* **1993**, *3*, 171.
(99) Foury-Leylekian, P.; Le Bolloc'h, D.; Hennion, B.; Ravy, S.; Moradpour, A.; Pouget, J. P. *Phys. Rev. B*, to be published.
(100) (a) Nad, F.; Monceau, P.; Carcel, C.; Fabre, J.-M *Phys. Rev.* **2000**, *B62*, 1753. (b) Monceau, P.; Nad, F. Y.; Brazovskii, S. *Phys. Rev. Lett.* **2001**, *86*, 4080.
(101) Chow, D. S.; Zamborsky, F.; Alavi, B.; Tantillo, D. J.; Baur, A.; Merlic, C. A.; Brown, S. E. *Phys. Rev. Lett.* **2000**, **85**, 1698.
(102) Brazovskii, S. *Synth. Met.* **2003**, *133*, 301.
(103) Javadi, H. H. S.; Laversanne, R.; Epstein, A. J. *Phys. Rev. B* **1988**, *37*, 4280.
(104) Laversanne, R.; Coulon, C.; Gallois, B.; Pouget, J.-P.; Moret, R. *J. Phys., Lett.* **1984**, *45*, L393.
(105) Foury-Leylekian, P.; Ravy, S.; Pouget, J.-P. *Physica B* **2002**, *312−313C*, 556.
(106) Ravy, S.; Foury-Leylekian, P.; Le Bolloc'h, D.; Pouget, J.-P. *J. Phys. IV* **2004**, *114*, 83.
(107) Nogami, Y.; Nakamura, T. *J. Phys. IV* **2002**, *12*, Pr9−145.
(108) Michel, P.; Moradpour, A.; Penven, P.; Firlej, L.; Bernier, P.; Levy, B.; Ravy, S.; Zahab, A. *J. Am. Chem. Soc.* **1990**, *112*, 8285.
(109) Ilakovac, V.; Ravy, S.; Moradpour, S.; Firlej, L.; Bernier, P. *Phys. Rev. B* **1995**, *52*, 4108.
(110) Hiraki, K.; Kanoda, K. *Phys. Rev. Lett.* **1998**, *80*, 4737.
(111) Miyagawa, K.; Kawamoto, A.; Kanoda, K. *Phys. Rev. B* **2000**, *62*, 7679.
(112) Watanabe, M.; Noda, Y.; Nogami, Y.; Oshima, K.; Mori, H. *J. Phys. IV* **2002**, *12*, Pr9−231.
(113) Seo, H.; Fukuyama, H. *Synth. Met.* **2003**, *133*, 257.
(114) Takano, Y.; Hiraki, K.; Yamamoto, H. M.; Nakamura, T.; Takahashi, T. *J. Phys. Chem. Solids* **2001**, *62*, 393.
(115) Nogami, Y.; Mori, T. *J. Phys. IV* **2002**, *12*, Pr9−233.
(116) Ilakovac, V.; Ravy, S.; Pouget, J.-P.; Lenoir, C.; Boubekeur, K.; Batail, P.; Dolanski Babic, S.; Biškup, N.; Korin-Hamzic, B.; Tomic, S.; Bourbonnais, C. *Phys. Rev. B* **1994**, *50*, 7136.
(117) Heuzé, K.; Fourmigué, M.; Batail, P.; Coulon, C.; Clérac, R.; Canadell, E.; Auban-Senzier, P.; Ravy, S.; Jérome, D. *Adv. Mater.* **2003**, *15*, 1251−1254.
(118) Leung, P. C. W.; Schultz, A. J.; Wang, H. H.; Emge, T. J.; Ball, G. A.; Cox, D. D.; Williams, J. M. *Phys. Rev. B* **1984**, *30*, 1615.
(119) Parkin, S. S. P.; Mayerle, J. J.; Engler, E. M. *J. Phys., Colloq.* **1983**, *44*, C3−1105.
(120) Pouget, J.-P.; Shirane, G.; Bechgaard, K.; Fabre, J.-M. *Phys. Rev. B* **1983**, *27*, 5203.
(121) Moret, R.; Pouget, J.-P.; Comès; Bechgaard, K. *J. Phys., Colloq.* **1983**, *44*, C3−957.
(122) Parkin, S. S. P.; Coulon, C.; Moret, R.; Pouget, J.-P. *Phys. Rev. B* **1987**, *36*, 2246.
(123) Ravy, S.; Pouget, J.-P.; Moret, R.; Wudl, F. *J. Phys. I* **1991**, *1*, 703.
(124) Coulon, C.; Maaroufi, A.; Amiell, J.; Duppart, E.; Flandrois, S.; Delhaes, P.; Moret, R.; Pouget, J.-P.; Morand, J.-P. *Phys. Rev. B* **1982**, *26*, 6322.
(125) Mortensen, K.; Tomkiewidz, Y.; Schultz, T. D.; Engler, E. M. *Phys. Rev. Lett.* **1981**, *46*, 1234.
(126) Torrance, J. B.; Pedersen, H. J.; Bechgaard, K. *Phys. Rev. Lett.* **1982**, *49*, 881.
(127) Le, L. P.; et al. *Europhys. Lett.* **1991**, *15*, 547; *Phys. Rev. B* **1993**, *48*, 7284.
(128) Pouget, J.-P.; Ravy, S. *Synth. Met.* **1997**, *85*, 1523.
(129) Delrieu, J. M.; Roger, M.; Toffano, Z.; Moradpour, A.; Bechgaard, K. *J. Phys. (Paris)* **1986**, *47*, 839.
(130) Takahashi, T.; Maniwa, Y.; Kawamura, H.; Saito, G. *J. Phys. Soc. Jpn.* **1986**, *55*, 1364.
(131) Tomic, S.; Cooper, J. R.; Kang, W.; Jérome, D.; Maki, K. *J. Phys. (Paris)* **1991**, *1*, 1603.
(132) Odin, J.; Lasjaunias, J. C.; Biljakovic, K.; Monceau, P.; Bechgaard, K. *Solid State Commun.* **1994**, *91*, 523.
(133) Blume, M. *J. Appl. Phys.* **1985**, *57*, 3615.
(134) Hill, J. P.; Helgensenet, G.; Gibbs, D. *Phys. Rev. B* **1995**, *51*, 10336 and references therein.
(135) Overhauser, A. W. *Phys. Rev.* **1992**, *167*, 8663.
(136) Foury-Leylekian, P.; Ravy, S.; Pouget, J.-P.; Müller, H. *Synth. Met.* **2003**, *137*, 1271.
(137) Kagoshima, S.; Saso, Y.; Maesato, M.; Kondo, R.; Hasegawa, T. *Solid State Commun.* **1999**, *110*, 479.
(138) (a) Kobayashi, N.; Ogata, M. *J. Phys. Soc. Jpn* **1997**, *66*, 3356. (b) Kobayashi, N.; Ogata, M.; Yonemitsu, K. *J. Phys. Soc. Jpn.* **1998**, *67*, 1098.
(139) Seo, H.; Fukuyama, H. *J. Phys. Soc. Jpn.* **1997**, *66*, 1249.
(140) Tomio, Y.; Suzumura, Y. *J. Phys. Soc. Jpn.* **2000**, *69*, 796.
(141) Liu, Q.; Ravy, S.; Pouget, J.-P.; Coulon, C.; Bourbonnais, C. *Synth. Met.* **1993**, *56*, 1840.
(142) Dumoulin, B.; Bourbonnais, C.; Ravy, S.; Pouget, J.-P.; Coulon, C. *Phys. Rev. Lett.* **1996**, *76*, 1360.
(143) Schulz, H. J. Unpublished results, quoted in ref 144.
(144) Pouget, J.-P. *Eur. Phys. J. B* **2001**, *20*, 321.
(145) Braden, M.; Hennion, B.; Reichardt, W.; Dhalenne, G.; Revcolevschi, A. *Phys. Rev. Lett.* **1998**, *80*, 3634.
(146) Valade, L. Ph.D. Thesis, Université Paul Sabatier, Toulouse, France, 1987.
(147) Bousseau, M.; Valade, L.; Legros, J. P.; Cassoux, P.; Garbauskas, M.; Interrante, L. V. *J. Am. Chem. Soc.* **1986**, *108*, 1908.
(148) Legros, J. P.; Valade, L. *Solid State Commun.* **1988**, *68*, 599.
(149) Kim, H.; Kobayashi, A.; Sasaki, Y.; Kato, R.; Kobayashi, H. *Chem. Lett.* **1987**, 1799.
(150) Clark, R. A.; Underhill, A. E. *Synth. Met.* **1988**, *27*, B515.
(151) Brossard, L.; Ribault, M.; Valade, L.; Cassoux, P. *J. Phys. (Paris)* **1989**, *50*, 1521.
(152) Auban, P.; Jérome, D.; Lestrup, K.; Johannsen, I.; Jorgensen, M.; Bechgaard, K. *J. Phys. (Paris)* **1989**, *50*, 2727.
(153) Gotschy, B.; Auban-Senzier, P.; Farall, A.; Bourbonnais, C.; Jérome, D.; Canadell, E.; Henriques, R. T.; Johannsen, I.; Bechgaard, K. *J. Phys. I* **1992**, *2*, 677.
(154) Moret, R.; Ravy, S.; Pouget, J.-P.; Comès, R.; Bechgaard, K. *Phys. Rev. Lett.* **1986**, *57*, 1915.
(155) Ravy, S.; Pouget, J.-P.; Valade, L.; Legros, J.-P. *Europhys. Lett.* **1989**, *9*, 391.
(156) Canadell, E.; Rachidi, I. E. I.; Ravy, S.; Pouget, J.-P.; Brossard, L.; Legros, J. P. *J. Phys. (Paris)* **1989**, *50*, 2967.
(157) Canadell, E.; Ravy, S.; Pouget, J.-P.; Brossard, L. *Solid State Commun.* **1990**, *75*, 633.
(158) Underhill, A. E.; Clark, R. A.; Mardsen, I.; Allan, M.; Friend, R. H.; Tajima, H.; Naito, T.; Tamura, M.; Kuruoda, H.; Kobayashi, A.; Kobayashi, H.; Canadell, E.; Ravy, S.; Pouget, J.-P. *J. Phys.: Condens. Matter* **1991**, *3*, 933.
(159) Liu, Q.; Ravy, S.; Pouget, J.-P.; Johannsen, I.; Bechgaard, K. *J. Phys. I* **1993**, *3*, 803.
(160) Liu, Q.; Ravy, S.; Pouget, J.-P.; Johannsen, I.; Bechgaard, K. *J. Phys. I* **1993**, *3*, 821.
(161) Ilakovac, V.; Ravy, S.; Boubekeur, K.; Lenoir, C.; Batail, P.; Pouget, J.-P. *Phys. Rev. B* **1997**, *56*, 13878.
(162) Nattermann, T.; Villain, J. *Phase Transitions* **1988**, *11*, 5.
(163) For a book on RFIM see: Young, A. P. *Spin Glasses and Random Fields*; World Scientific: London, 1998; p 387.
(164) Belanger, T. *Phase Transitions* **1988**, *11*, 53.
(165) Edwards, S. F.; Anderson, P. W. *J. Phys. F* **1975**, *5*, 965.
(166) Sherrington, D.; Kirkpatrick, S. *Phys. Rev. Lett.* **1975**, *35*, 1792.
(167) Dobrosavljevic, V.; Stratt, R. M. *Phys. Rev. B* **1987**, *36*, 8434.
(168) Tomic, S.; Jerome, D.; Mailly, D.; Ribault, M.; Bechgaard, K. *J. Phys., Colloq.* **1983**, *44*, C3−1073.
(169) Pouget, J.-P.; Kagoshima, S.; Tamegai, T.; Nogami, Y.; Kubo, K.; Nakajima, T.; Bechgaard, K. *J. Phys. Soc. Jpn.* **1990**, *59*, 2036.
(170) Monceau, P.; Ong, N. P.; Portis, A. M.; Meerschaut, A.; Rouxel, J. *Phys. Rev. Lett.* **1976**, *37*, 602.
(171) Dumas, J.; Schlenker, C.; Marcus, J.; Buder, R. *Phys. Rev. Lett.* **1983**, *50*, 757.

(172) Tomic, S.; Cooper, J. R.; Jrome, D.; Bechgaard, K. *Phys. Rev. Lett.* **1989**, *62*, 462.
(173) Imry, Y.; Ma, S. K. *Phys. Rev. Lett.* **1975**, *35*, 1400.
(174) Imbrie, J. Z. *Phys. Rev. Lett.* **1984**, *53*, 1747.
(175) Binder, Z. *Phys. B* **1983**, *50*, 343.
(176) Fukuyama, H. *J. Phys. Soc. Jpn.* **1973**, *41*, 513.
(177) Fukuyama, H.; Lee, P. A. *Phys. Rev. B* **1978**, *17*, 535.
(178) Lee, P. A.; Rice, T. M. *Phys. Rev. B* **1979**, *19*, 3970.
(179) For a recent review see: *Adv. Phys.* **2004**, *53*, 177.
(180) Larkin, A. I.; Ovchinikov, Y. N. *J. Low. Temp. Phys.* **1979**, *34*, 409.
(181) Nattermann, T.; Scheidl, S. *Adv. Phys.* **2000**, *49*, 607.
(182) Nattermann, T. *Phys. Rev. Lett.* **1990**, *64*, 2454.
(183) Korshunov, S. E. *Phys. Rev. B* **1993**, *48*, 3969.
(184) Giamarchi, T.; Le Doussal, P. *Phys. Rev. B* **1995**, *52*, 1242.
(185) Giamarchi, T.; Le Doussal, P. In *Spin Glasses and Random Fields*; Young, A. P., Ed.; World Scientific: Singapore, 1998; p 321. Also in cond-mat/9705096.
(186) Friedel, J. *Philos. Mag.* **1952**, *43*, 153; *Adv. Phys.* **1954**, *3*, 446; *Nuovo Cimento, Suppl.* **1958**, *87*, 287.
(187) Ravy, S.; Requardt, H.; Le Bolloc'h, D.; Foury-Leylekian, P.; Pouget, J.-P.; Currat, R.; Monceau, P.; Krisch, M. *Phys. Rev. B* **2004**, *69*, 115113.
(188) Rouzière, S.; Ravy, S.; Pouget, J.-P.; Brazovskii, S. *Phys. Rev. B* **2000**, *62*, R16231.
(189) Abe, S. *J. Phys. Soc. Jpn.* **1985**, *54*, 3498; **1986**, *55*, 1987.
(190) Bâldea, I. *Phys. Rev. B* **1995**, *51*, 1495. Bâldea, I.; Köppel, H.; Cederbaum, L. *Phys. Rev. B* **1995**, *52*, 11845.
(191) Larkin, A. I.; Brazovskii, S. *Solid State Commun.* **1995**, *93*, 275.
(192) Tüttö, I.; Zawadowski, A. *Phys. Rev. B* **1985**, *32*, 2449.
(193) Tucker, J. R. *Phys. Rev. B* **1989**, *40*, 5447.
(194) Sham, L. J.; Patton, B. R. *Phys. Rev. B* **1976**, *13*, 3151.
(195) Debye, P.; Anderson, H. R., Jr.; Brumberger, H. *J. Appl. Phys.* **1957**, *38*, 679.
(196) Girault, S.; Moudden, A. H.; Pouget, J.-P.; Godard, J.-M. *Phys. Rev. B* **1988**, *38*, 7980.
(197) Rouzière, S.; Ravy, S.; Brazovskii, S.; Pouget, J.-P. *J. Phys. IV***1999**, *9*, Pr10−23.
(198) DeLand, S.; Mozurkewich, G.; Chapman, L. D. *Phys. Rev. Lett.* **1991**, *66*, 2026.
(199) Sweetland, E.; Finnefrock, A. C.; Podulka, W. J.; Sutton, M.; Brock, J.; Dicarlo, D.; Thorne, R. E. *Phys. Rev. Lett.* **1990**, *65*, 3165.
(200) Brock, J. D.; Finnefrock, A. C.; Ringland, K. L.; Sweetland, E. *Phys. Rev. Lett.* **1994**, *73*, 3588.
(201) DiCarlo, D.; Thorne, R. E.; Sweetland, E.; Sutton, M.; Brock, J. D. *Phys. Rev. B* **1994**, *50*, 8288.
(202) DiCarlo, D. A.; McCarten, J.; Adelman, T. L.; Maher, M.; Thorne, R. E. *Phys. Rev. B* **1990** *42*, 7643. McCarten, J.; DiCarlo, D. A.; Maher, M. P.; Adelman, T. L.; Thorne, R. E. *Phys. Rev. B* **1992**, *46*, 4456.
(203) Stephenson, J. *Can. J. Phys.* **1969**, *47*, 2621; **1970** *48*, 1724.
(204) Garel, T.; Maillard, J. M. *J. Phys. C* **1986**, *19*, L505.
(205) Garel, T.; Ilakovac, V.; Ravy, S. *Phys. Rev. B* **1994**, *49*, 12791.
(206) Enkelmann, V. *J. Phys., Colloq.* **1983**, *44*, C3, 1147.
(207) Mortensen, K.; Engler, E. M. *Phys. Rev. B* **1984**, *29*, 842.
(208) Coulon, C.; Delhaes, P.; Amiel, J.; Manceau, J. P.; Fabre, J.-M.; Giral, L. *J. Phys. (Paris)* **1982**, *43*, 1721.
(209) Emery, V. J.; Noguera, C. *Phys. Rev. Lett.* **1988**, *60*, 631.
(210) Ravy, S.; Pouget, J.-P.; Comès, R. *J. Phys. I* **1992**, *2*, 1173.
(211) Ravy, S.; Pouget, J.-P. *J. Phys. IV* **1993**, *3*, 109.
(212) Welberry, T. R.; Fox, N. J. *J. Appl. Crystallogr.* **1995**, *28*, 611.
(213) Rosso, A.; Giamarchi, T. *Phys. Rev. B* **2003**, *68*, 140201.

CR030662H